LETTERS
https://doi.org/10.1038/s41591-019-0598-9
nature medicine

A luminal unfolding microneedle injector for oral delivery of macromolecules

Alex Abramson[1,2,13], Ester Caffarel-Salvador[1,2,3,13], Vance Soares[1,2], Daniel Minahan[1,2], Ryan Yu Tian[1,2], Xiaoya Lu[1,2], David Dellal[2,3], Yuan Gao[1,2], Soyoung Kim[1,2], Jacob Wainer[1,2], Joy Collins[1,2], Siddartha Tamang[1,2], Alison Hayward[1,2,4], Tadayuki Yoshitake[5,6], Hsiang-Chieh Lee[5,6], James Fujimoto[5,6], Johannes Fels[7,8], Morten Revsgaard Frederiksen[7,8], Ulrik Rahbek[7,8], Niclas Roxhed[1,2,9], Robert Langer[1,2,3,10,11]* and Giovanni Traverso[1,2,10,12]*

Insulin and other injectable biologic drugs have transformed the treatment of patients suffering from diabetes[1,2], yet patients and healthcare providers often prefer to use and prescribe less effective orally dosed medications[3–5]. Compared with subcutaneously administered drugs, oral formulations create less patient discomfort[4], show greater chemical stability at high temperatures[6], and do not generate biohazardous needle waste[7]. An oral dosage form for biologic medications is ideal; however, macromolecule drugs are not readily absorbed into the bloodstream through the gastrointestinal tract[8]. We developed an ingestible capsule, termed the luminal unfolding microneedle injector, which allows for the oral delivery of biologic drugs by rapidly propelling dissolvable drug-loaded microneedles into intestinal tissue using a set of unfolding arms. During ex vivo human and in vivo swine studies, the device consistently delivered the microneedles to the tissue without causing complete thickness perforations. Using insulin as a model drug, we showed that, when actuated, the luminal unfolding microneedle injector provided a faster pharmacokinetic uptake profile and a systemic uptake >10% of that of a subcutaneous injection over a 4-h sampling period. With the ability to load a multitude of microneedle formulations, the device can serve as a platform to orally deliver therapeutic doses of macromolecule drugs.

Since insulin was first injected into a human subject in 1922, scientists have explored methods to formulate biologic macromolecules for oral delivery[9]. More recently, instead of focusing on reformulation, we and others have conducted initial feasibility evaluations of capsule-mediated injections in the gastronintestinal tract[10–12]. Previously, we demonstrated the ability to deliver macromolecule drugs via a capsule-based injection to the stomach[10]. Additionally, human tolerability studies of capsule-mediated injections[12] in the small intestine and endoscopic insulin injections through this route[11] support the feasibility of capsule-based injection systems targeting the small intestine.

Diffusion across the mucus and tissue layers of the gastrointestinal tract, and enzymatic degradation, fundamentally limit undigested biomacromolecule absorption[13]. Researchers have developed permeation enhancers[14,15], nanoparticle encapsulations[16,17] and mucus adhering patches[18] to enhance biomacromolecule uptake. However, these innovations dampen pharmacokinetics[15,18] and reduce bioavailability[19] compared with dosing via parenteral routes. To address these problems, we created an orally dosed device that physically inserts drug-loaded microneedles into the small intestine, bypassing the need for diffusion into the tissue wall. The device holds a clinically relevant drug load, provides faster systemic uptake after actuation, and has a systemic bioavailability >10% of that of a subcutaneous injection over a 4-h sampling period.

The luminal unfolding microneedle injector (LUMI) pill utilizes the tube-like geometry of the small intestine to create multiple points of contact with the tissue (Fig. 1a–e; see Extended Data Fig. 1). Each of the device's three degradable arms stretches the tissue and propels a patch of 1-mm-long, dissolving drug-loaded microneedles into the tissue wall. We optimized the force from the LUMI's elastomer and spring steel core to ensure microneedle penetration while avoiding perforation (Fig. 1f–k; see Extended Data Fig. 2).

We designed a custom capsule measuring 9 mm in diameter and 30 mm in length that allowed the LUMI to remain separated from fluid until seconds before actuation, preventing microneedle dissolution before insertion (Fig. 1a; see Extended Data Fig. 3). The capsule utilized a poly(methacrylic acid-co-ethyl acrylate) coating, designed to dissolve at a pH of ≥5.5, in combination with a polyethylene glycol (PEG) (molecular weight: 3,500) coating to encapsulate a compressed spring that propelled the LUMI out of the capsule. We demonstrated in vitro that changing the molecular weight of the PEG coating could delay the actuation of the capsule from 1–5 h after entering an environment with a pH of ≥5.5 (Fig. 1l). After actuation, the capsule broke apart into fenestrated pieces ≤9 mm in diameter and 15 mm in length, to enable safe passage through the gastrointestinal tract. The fenestrations allow chyme to pass through. Although the risk of small intestinal obstruction

[1]Department of Chemical Engineering, Massachusetts Institute of Technology, Cambridge, MA, USA. [2]David H. Koch Institute for Integrative Cancer Research, Massachusetts Institute of Technology, Cambridge, MA, USA. [3]Institute for Medical Engineering and Science, Massachusetts Institute of Technology, Cambridge, MA, USA. [4]Division of Comparative Medicine, Massachusetts Institute of Technology, Cambridge, MA, USA. [5]Department of Electrical Engineering and Computer Science, Massachusetts Institute of Technology, Cambridge, MA, USA. [6]Research Laboratory of Electronics, Massachusetts Institute of Technology, Cambridge, MA, USA. [7]Global Research Technologies, Global Drug Discovery, Måløv, Denmark. [8]Device R&D, Novo Nordisk, Måløv, Denmark. [9]Department of Micro and Nanosystems, KTH Royal Institute of Technology, Stockholm, Sweden. [10]Department of Mechanical Engineering, Massachusetts Institute of Technology, Cambridge, MA, USA. [11]Media Lab, Massachusetts Institute of Technology, Cambridge, MA, USA. [12]Division of Gastroenterology, Brigham and Women's Hospital, Harvard Medical School, Boston, MA, USA. [13]These authors contributed equally: Alex Abramson, Ester Caffarel-Salvador. *e-mail: rlanger@mit.edu; cgt20@mit.edu

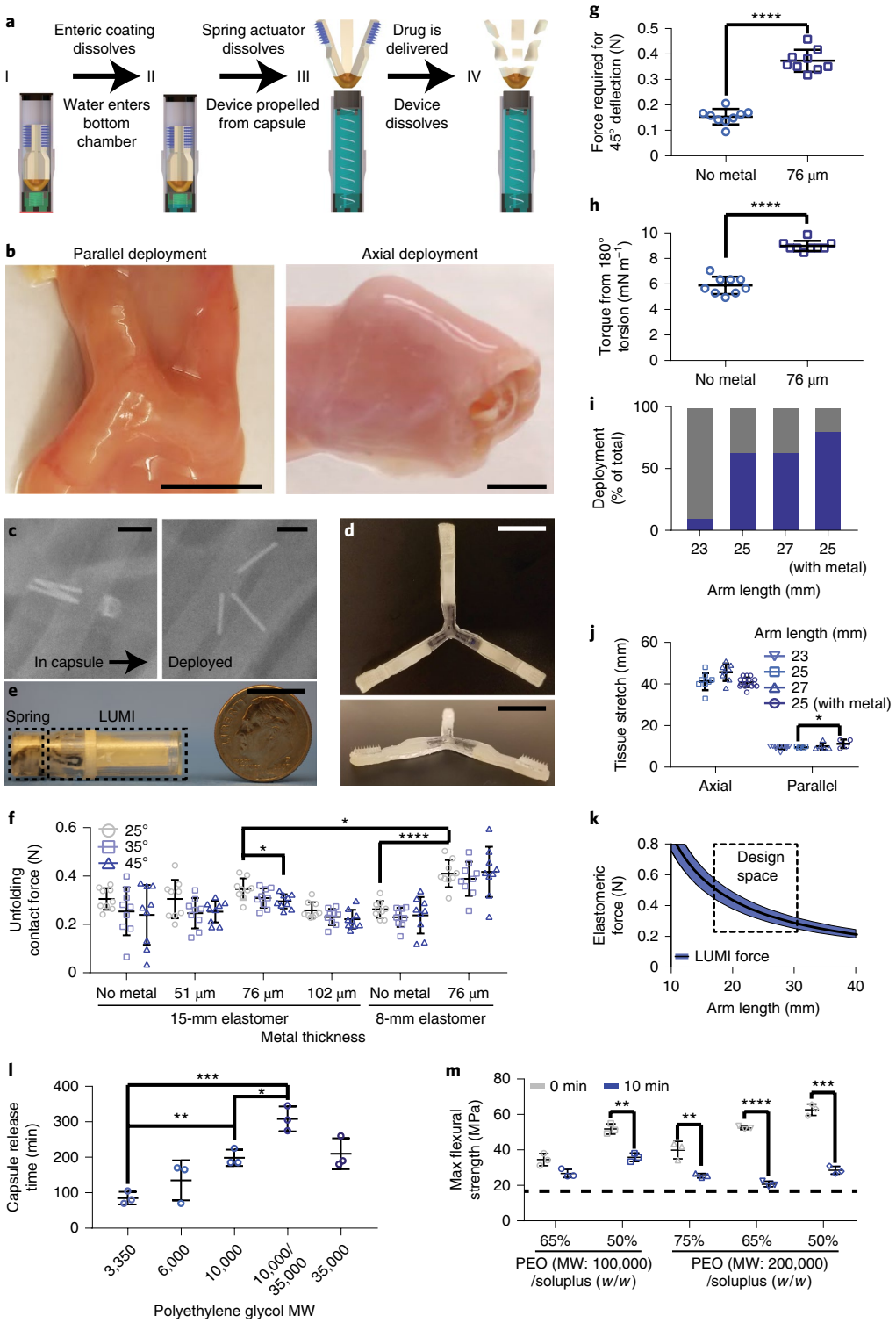

Fig. 1 | LUMI fabrication and design specifications. a, LUMI actuation scheme. **b**, LUMI devices opened in multiple orientations in the small intestine, including in the parallel (left) or axial directions (right) shown here. **c**, Radiographs confirming capsule actuation in vivo in the swine within 2 h. Metal rods were used for imaging purposes, and were not part of the final design. **d**, Overhead (top) and side-view (bottom) images of an unfolded LUMI. **e**, Encapsulated LUMI. **f**, Mean ± s.d. unfolding contact force applied by the LUMI arm in vitro ($n = 9$ device replicates). **g**,**h**, Mean ± s.d. forces required for arm deflection (**g**) and torsion (**h**) in vitro ($n = 9$ device replicates). **i**, Percentages of devices deployed axially in vivo in the swine (blue) versus parallel (gray) ($n = 15$ technical replicates). **j**, Mean ± s.d. tissue stretch from unfolding in vivo in the swine ($n = x$ device replicates on one animal replicate (25 mm axial: $n = 8$; 27 mm axial: $n = 8$; 25 mm axial (with metal): $n = 15$; 23 mm parallel: $n = 10$; 25 mm parallel: $n = 5$; 27 mm parallel: $n = 5$; 25 mm parallel (with metal): $n = 4$)). **k**, LUMI design space based on arm length and the elastomeric force beneficial for administration. **l**, Mean ± s.d. in vitro capsule release time ($n = 3$ device replicates). MW, molecular weight. 10,000/35,000 represents a 50/50 (w/w) mixture of the two molecular weight polymers. **m**, Mean ± s.d. arm flexural strength before and after dissolution in simulated intestinal fluid at 37 °C in vitro. The dashed line represents the calculated flexural stress required to break the LUMI arm ($n = 3$ device replicates). $^{*}P < 0.05$; $^{**}P < 0.01$; $^{***}P < 0.001$; $^{****}P < 0.0001$. Scale bars: 1 cm.

increases with the presence of large, non-degradable objects in the gastrointestinal lumen, the hazard is mitigated with smaller objects. The LUMI utilized osmotic-controlled release oral delivery system (OROS) osmotic pump capsules (9 mm in diameter and 15 mm in length; or 12 mm in diameter and 5 mm in length)—daily dosed and non-degrading drug delivery devices approved by the Food and Drug Administration (FDA)—as models to guide the sizes of the device and individual components. OROS devices show obstruction rates of approximately 1 in 39 million or less[20].

When exiting the capsule, the LUMI can open in any orientation relative to the small intestine. We specifically studied the deployment from two orientations: axially symmetric or parallel to the central axis of the small intestine (Fig. 1b). These two orientations were the alignments at which the LUMI provided the greatest and least amount of tissue stretching, respectively. A geometric analysis of all opening events (see Methods) allowed us to design the LUMI with an arm length long enough to ensure that the microneedles always made contact with, conformed around and stretched the tissue wall, regardless of the LUMI's orientation within the small intestine. Nevertheless, devices were optimized via in vivo experiments to orient most frequently in the axial direction, to provide the greatest amount of force for microneedle insertion.

We designed the LUMI device's unfolding arms to maintain sufficient strength after actuation, to deliver the drug payload in vivo, while still dissolving in a timely manner to prevent obstruction. Fabricated from mixtures of biodegradable polyethylene oxide (PEO) and Soluplus (polyvinyl caprolactam-polyvinyl acetate-polyethylene glycol graft copolymer), the arms degraded within 24 h in vitro and in vivo (see Extended Data Fig. 4); however, the arms retained enough mechanical strength 10 min into degradation to remain intact and push microneedles against the tissue wall, as determined via a three-point bend test in vitro (Fig. 1m). Spacing between the arms allowed for chyme to pass around the device and mitigate the risk of obstruction while the LUMI was in an unfolded state.

The non-degradable elastomeric core of the LUMI, measuring 12 mm in diameter and 1.5 mm in height, passed through the gastrointestinal tract along with the capsule parts without issue during all of the in vivo experiments. In one experiment, we fed a total of 12 capsules and 12 LUMI devices to the stomachs of three different swine. Radiographs confirmed the passage and excretion of all devices, and at least one device was retrieved intact and examined after excretion from each swine. The eight devices not retrieved were lost in the cage bedding. We performed upper and lower endoscopies on the animals after the devices were excreted, and we saw no abnormalities in the sections of the upper and lower gastrointestinal tract that were endoscopically evaluable. Moreover, at the time of euthanasia, the entire gastrointestinal tracts of all of the animals were examined; no gross abnormalities caused by the devices were observed, and no devices remained inside the body.

After characterizing the device, we designed microneedle patches to enable rapid drug delivery of clinically relevant doses (Fig. 2). We performed penetration experiments on ex vivo human small intestine tissue, as well as on ex vivo and in vivo swine tissue, to determine the force and distance required for needle penetration while avoiding a full-thickness perforation (Fig. 2g,h; see Extended Data Fig. 5). Force measurements showed that beveled, stainless steel needles entered the tissue after applying as low as 5 mN of force (see Supplementary Video 1). The needles reached a displacement of over 6 mm before perforating the outermost tissue layer. Perforation forces for a single needle into in vivo swine tissue ranged from 0.27–0.53 N, compared with 0.20–0.28 N for ex vivo human tissue perforation. This suggests that perforation could be mitigated by limiting the applied force and the height of the needles used in the LUMI.

Using these results, we designed the LUMI to deliver patches containing 32 conical, drug-loaded, polymeric microneedles on each arm. Microneedles were fabricated to be 1 mm in height. The simultaneous delivery of multiple microneedles dispersed the applied force ('bed-of-needles' effect), and the microneedle height limited the ability for the device to perforate the tissue. To ensure penetration, the LUMI arms applied a contact force measuring 0.41 ± 0.06 N, or 13 mN per microneedle. Of note, microneedle applicators disproportionately apply force across the patch[21], and the small intestine possesses an uneven surface due to folds and villi projections, making the tissue more susceptible to uneven force distributions; however, multiple imaging techniques confirmed LUMI microneedle penetration into ex vivo and in vivo small intestine tissue with no full-thickness perforation. Microcomputed tomography (microCT) images of LUMIs loaded with barium sulfate microneedle patches (Fig. 2c) and hypodermic needles (see Extended Data Fig. 6) showed tissue penetration in ex vivo small intestine tissue without perforation, as denoted by the dotted lines. These results were further supported using histology, where LUMI-deployed hypodermic needles coated with tissue-marking dye penetrated 800 µm through the tissue (Fig. 2e). The absence of dye in the 1-mm section suggested that the needle did not reach this depth, supporting its probable inability to perforate the small intestine. Optical coherence tomography (OCT) also confirmed microneedle penetration after the manual insertion of a patch (Fig. 2i) or deployment of a single LUMI arm into the tissue from a 30° angle (see Extended Data Fig. 7). To demonstrate microneedle penetration in vivo and assess the effects of needle insertion on live tissue, histology was taken after dosing to sedated swine (Fig. 3). As a control, microneedle insertion was compared with insertion of a 32-G beveled, stainless steel needle coated in blue tissue-marking dye. One factor to consider when exploring tissue penetration and perforation characteristics is the age of the patient receiving the device, as the risk of bowel perforation is known to increase with age[22]. We performed our human tissue needle penetration characterization studies on samples from patients aged 32, 45 and 70 years (see Supplementary Table 1) and used the information from all three samples to determine the LUMI device design specifications.

Each LUMI held up to 0.3 mg of drug in a total microneedle footprint area of 0.5 cm^2. API powder was used to raise the drug loading fraction in the microneedle patch (Fig. 2a), which was then incorporated into the LUMI arm in an outward configuration (Fig. 2b), with an indentation in the arm to prevent needle breakage during encapsulation. We demonstrated the ability of the LUMI to load multiple APIs by incorporating microneedle patches made with insulin, lysozyme and α-glucosidase (see Extended Data Fig. 8). These included patches that used either polyvinylpyrrolidone or sorbitol as a binding ingredient. Microneedle dissolution and drug delivery kinetics were studied in vitro (Fig. 2d,f,i; see Extended Data Fig. 9) before in vivo evaluation.

LUMI devices loaded with recombinant human insulin were deployed in vivo into swine jejunum, and a peak plasma human insulin concentration was observed approximately 25 min after actuation, with associated hypoglycemia (Fig. 4). LUMI device deployment was compared with subcutaneous injection of a dissolved microneedle patch, administration of a dissolved patch into the jejunum lumen, and manual application of the microneedle patch into the jejunum wall. During each set of swine trials, 1 cm^2 of microneedle patch was loaded with 0.6 mg human insulin and delivered to each swine ($n = 3$ animal replicates). LUMI-dosed swine received two devices to achieve this dose. During filtration for the subcutaneous dosing, some of the insulin was lost in the filter, and the final calculated insulin dose was 0.2 mg. The LUMI method of delivery provided a 44 ± 5% decrease in blood glucose

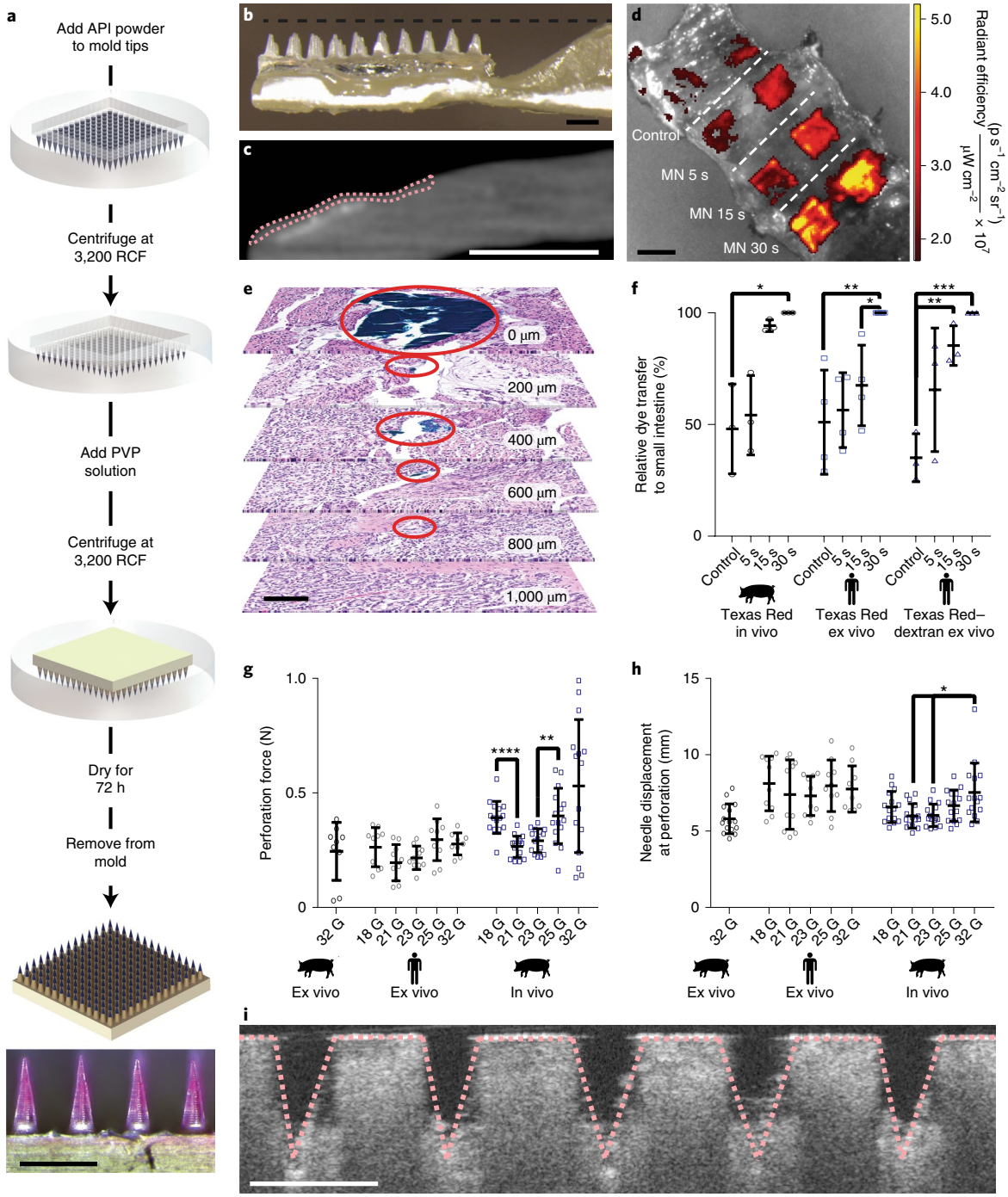

Fig. 2 | Microneedle characterization in the small intestine. a, Polyvinylpyrrolidone (PVP) microneedles (MNs) fabricated using solid API powder. One patch (1 cm^2) held up to 0.6 mg API in the tips alone. The patch pictured below contains Texas Red fluorescent dye. Scale bar: 1 mm. **b**, The LUMI arm indentation houses insulin-loaded MNs during encapsulation. Scale bar: 1 mm. **c**, MicroCT image of a barium sulfate-loaded MN patch applied to a section of human small intestine using LUMI (axially symmetric deployment). The tissue is outlined. Scale bar: 5 mm. **d**, In Vivo Imaging System fluorescence image of Texas Red MN dissolution in human tissue. Scale bar: 10 mm. **e**, Histology confirming needle penetration without perforation using LUMI in ex vivo small intestine tissue. Blue surgical dye, used to coat the needle, reached 800 μm below the surface of the tissue. Scale bar: 0.1 mm. **f**, Mean ± s.d. relative dye transfer of MNs to small intestine tissue over time ($n = x$ biologic replicates (swine Texas Red: $n = 3$ animal replicates; human Texas Red: $n = 4$ patient replicates; human Texas Red-dextran: $n = 3$ patient replicates)). **g**,**h**, Mean ± s.d. force (**g**) and displacement (**h**) required for beveled, stainless steel needle perforation in the small intestine (swine: $n = 5$ technical replicates each for $n = 3$ animal replicates, totaling $n = 15$ (for 32 G force, $n = 3$ technical replicates for $n = 3$ animal replicates, totaling $n = 9$); human: $n = 3$–4 technical replicates each for $n = 3$ patient replicates, totaling $n = 10$ (for 32 G, $n = 3$ technical replicates for $n = 3$ patient replicates, totaling $n = 9$)). **i**, OCT confirmed that MNs penetrated into the small intestine tissue ex vivo. Scale bar: 1 mm. $^*P < 0.05$; $^{**}P < 0.01$; $^{***}P < 0.001$; $^{****}P < 0.0001$.

over 60 min, and all LUMI trials showed insulin uptake (Fig. 4b) and a decrease in blood glucose (Fig. 4a). Comparably, subcutaneous injection and small intestine patch application produced decreases in blood glucose of 64 ± 12 and 54 ± 8%, respectively. However, when the solution with solubilized microneedles was administered into the jejunal lumen, the swine showed no significant blood

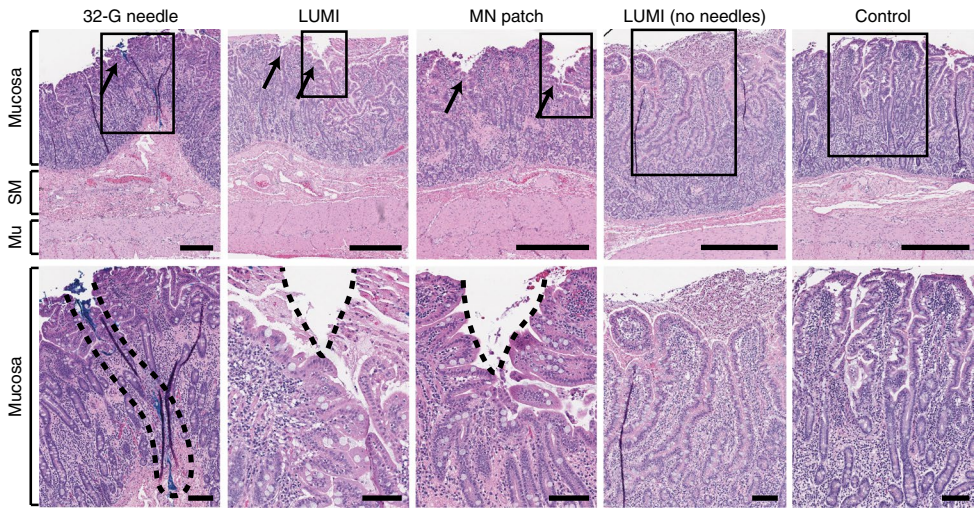

Fig. 3 | Small intestine histology after device actuation. Hematoxylin and eosin-stained small intestine tissues from swine, taken at the site of actuation. Bottom: magnification of the sections of the top images that are highlighted by black rectangles. The 32-G hypodermic needle was coated in surgical dye, which acted as a surrogate for the needle insertion depth, as no hole in the tissue was seen. Mu, muscularis externa; SM, submucosa. Scale Bars: 0.5 mm (top) and 0.1 mm (bottom). Arrows denote locations of needle penetration.

glucose level changes. Swine dosed with the LUMI devices experienced peak human insulin plasma concentrations faster than swine dosed subcutaneously. Over the sampling period, the swine dosed with LUMIs showed an average of more than 10% systemic uptake compared with those dosed subcutaneously (when taking into account the difference in dose), and 40% systemic uptake compared with those dosed with the manually applied microneedle patch (Fig. 4c, Supplementary Table 2).

While several safety concerns surround the process of injection in the gastrointestinal tract, retrospective analyses showed a tolerance for the action, and gastrointestinal tissue possesses some capability to regenerate tissue and recover after injury[23]. Gastroenterologists regularly employ a 5-mm-long 25-gauge needle to inject saline into the small intestine and colon wall[24]. Additionally, case studies on swallowed sharp objects, such as razor blades and needles, show that the small intestine safely withstands transiting sharp objects up to 1 cm in length[11,25]. While this incidence rate is too high for a daily dosed drug delivery vehicle, it suggests that there exists a window of safe operation for injection with smaller needles.

Because the LUMI stretched the small intestine, discomfort may have occurred due to bowel distention during actuation while the swine were anesthetized[26]. In our studies, we monitored the swine for one week following administration, and they showed no discomfort, change in feeding habit, or abnormal behavior in socializing. During future studies in awake animals, and in early clinical evaluation, we plan to monitor the severity and length of negative sensations, if any, due to LUMI expansion. Additionally, future long-term studies will be required to understand the effects of chronic injections into intestinal mucosa; however, during our studies, we observed only minimal damage to the mucosa and no signs of inflammation within five minutes after delivering the device. Furthermore, given the length of the small intestine, the LUMI may not consistently target the same area of tissue.

After exiting the body, non-degradable solid dosage forms approved by the FDA, such as the OROS system, are removed from the waste stream by sewage-treatment facilities[27,28]. Because the LUMI possesses a similar size and material make-up to these FDA-approved capsules, we anticipate that the LUMI would have a comparable FDA environmental assessment. Of note, the LUMI's metal components could interfere with magnetic resonance imaging machines. Hence, patients would need to disclose the intake of the pill during such procedures. Future versions of the system could be fabricated from other materials, including polymeric springs, to minimize the potential interactions with imaging modalities.

Importantly, the LUMI device relied on gastric emptying to move from the stomach to the small intestine. Gastric emptying typically occurs in 1–4 h, but can take up to 24 h in individuals experiencing gastroparesis, as is common in diabetic patients[29,30]. This variability leads to an uncertainty and a delay in the onset of drug action. Swine have previously been observed to possess exceedingly slow gastric transit times compared with humans and dogs[31]. For these reasons, we were unable to deliver the LUMI device to the stomach during our in vivo trials measuring drug pharmacokinetics; however, the capsule's enteric coating has been extensively tested in other studies[15,32], and we demonstrated in vivo the ability of capsules to pass from the stomach to the small intestine. Our pharmacokinetic studies showed fast hypoglycemic onset for insulin delivered via the small intestine, but this did not account for the gastric emptying time. The post-administration hypoglycemic onset time may be delayed by several hours as the device travels to the small intestine. We also showed that our capsule could release the LUMI after spending different amounts of time in the small intestine, potentially allowing us to tune the delivery time for patients with delayed or enhanced peristalsis.

Ultimately, the LUMI device showed consistent deployment into the small intestinal mucosa during preclinical in vivo swine studies. While recombinant human insulin was used as a model drug in the study, APIs with broader therapeutic windows and longer half-lives, such as long-acting insulin, may be better suited for LUMI-mediated delivery. Additionally, the LUMI could potentially load numerous biomacromolecules mentioned in the microneedle literature, including vaccines, monoclonal antibodies, enzymes, hormones, RNA and other compounds currently lacking oral formulations[33]. Macromolecule drugs that are not conducive to subdermal injection due to local skin reactions, such as oligonucleotides[34] and certain tumor necrosis factor-α inhibitors, would be particularly interesting targets to study. Further studies exploring a range of APIs are warranted, as clinical translation of orally delivered gastrointestinal microneedle injections could lead to a paradigm shift in macromolecule delivery.

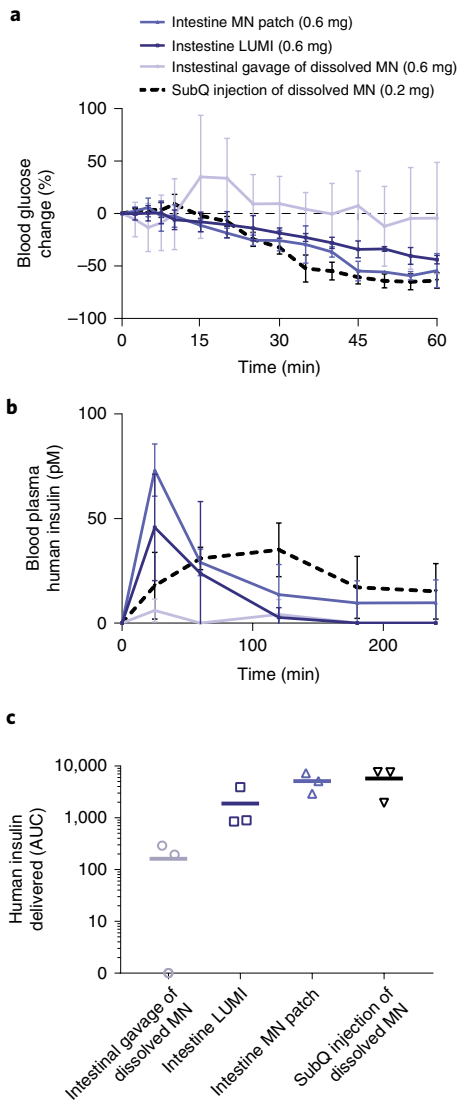

Fig. 4 | In vivo human insulin delivery via the LUMI in swine. **a**,**b**, Mean ± s.d. blood glucose (**a**) and plasma human insulin levels (**b**) ($n = 3$ animal replicates). Doses were delivered in one of the following ways: manual MN patch application to the jejunum (intestine MN patch); deployment of two LUMIs in the jejunum (intestine LUMI); dissolution in 0.5 ml sterile saline, filtration through a low protein binding sterilization filter, and administration subcutaneously (SubQ injection of dissolved MN); dissolution in 10 ml water and administration into the lumen of the jejunum via an endoscope (intestinal gavage of dissolved MN). Individual pharmacokinetics and pharmacodynamics profiles can be found in the attached source data file. **c**, Mean and individual animal replicate calculations for total plasma insulin (calculated using the area under the curve (AUC)) delivered by each method over a 4-h sampling period after administration ($n = 3$ animal replicates).

Online content

Any methods, additional references, Nature Research reporting summaries, source data, statements of code and data availability and associated accession codes are available at https://doi.org/10.1038/s41591-019-0598-9.

Received: 20 December 2018; Accepted: 28 August 2019;
Published online: 7 October 2019

References

1. Turner, R. C., Cull, C. A., Frighi, V. & Holman, R. R. Glycemic control with diet, sulfonylurea, metformin, or insulin in patients with type 2 diabetes mellitus: progressive requirement for multiple therapies (UKPDS 49). *J. Am. Med. Assoc.* **281**, 2005–2012 (1999).
2. Pratley, R. E. et al. Liraglutide versus sitagliptin for patients with type 2 diabetes who did not have adequate glycaemic control with metformin: a 26-week, randomised, parallel-group, open-label trial. *Lancet* **375**, 1447–1456 (2010).
3. Korytkowski, M. When oral agents fail: practical barriers to starting insulin. *Int. J. Obes.* **26**, S18–S24 (2002).
4. Boye, K. S. et al. Utilities and disutilities for attributes of injectable treatments for type 2 diabetes. *Eur. J. Heal. Econ.* **12**, 219–230 (2011).
5. Calvert, M. J., McManus, R. J. & Freemantle, N. Management of type 2 diabetes with multiple oral hypoglycaemic agents or insulin in primary care: retrospective cohort study. *Br. J. Gen. Pract.* **57**, 455–460 (2007).
6. Cleland, J. & Langer, R. in *Formulation and Delivery of Proteins and Peptides* (eds. Cleland, J. L. & Langer, R.) 1–19 (American Chemical Society, 1994).
7. Dallel, N., Kacem, M., Nabouli, R. M. & El May, M. Disposal of insulin syringes by diabetic patients. Report of 100 patients.*Tunis. Med.* **83**, 390–392 (2005).
8. Anselmo, A. C., Gokarn, Y. & Mitragotri, S. Non-invasive delivery strategies for biologics. *Nat. Rev. Drug Discov.* **18**, 19–40 (2018).
9. Harrison, G. A. Insulin in alcoholic solution by the mouth. *Br. Med. J.* **2**, 1204–1205 (1923).
10. Abramson, A. et al. An ingestible self-orienting system for oral delivery of macromolecules. *Science* **363**, 611–615 (2019).
11. Traverso, G. et al. Microneedles for drug delivery via the gastrointestinal tract. *J. Pharm. Sci.* **104**, 362–367 (2015).
12. Scudellari, M. Shot to the Gut: "Robotic" Pill Sails Through Human Safety Study. https://spectrum.ieee.org/the-human-os/biomedical/devices/shot-to-the-gut-robotic-pill-sails-through-human-safety-study (accessed 25 September 2019).
13. Vllasaliu, D., Thanou, M., Stolnik, S. & Fowler, R. Recent advances in oral delivery of biologics: nanomedicine and physical modes of delivery. *Expert Opin. Drug Deliv.* **15**, 759–770 (2018).
14. Davies, M. et al. Effect of oral semaglutide compared with placebo and subcutaneous semaglutide on glycemic control in patients with type 2 diabetes. *J. Am. Med. Assoc.* **318**, 1460–1470 (2017).
15. Banerjee, A. et al. Ionic liquids for oral insulin delivery. *Proc. Natl Acad. Sci. USA* **115**, 7296–7301 (2018).
16. Mathiowitz, E. et al. Biologically erodable microspheres as potential oral drug delivery systems. *Nature* **386**, 410–414 (1997).
17. Pridgen, E. M., Alexis, F. & Farokhzad, O. C. Polymeric nanoparticle drug delivery technologies for oral delivery applications. *Expert Opin. Drug Deliv.* **12**, 1459–1473 (2015).
18. Banerjee, A., Wong, J., Gogoi, R., Brown, T. & Mitragotri, S. Intestinal micropatches for oral insulin delivery. *J. Drug Target.* **25**, 608–615 (2017).
19. Mitragotri, S., Burke, P. A. & Langer, R. Overcoming the challenges in administering biopharmaceuticals: formulation and delivery strategies. *Nat. Rev. Drug Discov.* **13**, 655–672 (2014).
20. Bass, D. M., Prevo, M. & Waxman, D. S. Gastrointestinal safety of an extended-release, nondeformable, oral dosage form (OROS): a retrospective study. *Drug Saf.* **25**, 1021–1033 (2002).
21. Coffey, J. W., Meliga, S. C., Corrie, S. R. & Kendall, M. A. F. Dynamic application of microprojection arrays to skin induces circulating protein extravasation for enhanced biomarker capture and detection. *Biomaterials* **84**, 130–143 (2016).
22. Gatto, N. M. et al. Risk of perforation after colonoscopy and sigmoidoscopy: a population-based study. *J. Natl Cancer Inst.* **95**, 230–236 (2003).
23. Podolsky, D. K. Healing the epithelium: solving the problem from two sides. *J. Gastroenterol.* **32**, 122–126 (1997).
24. Classen, M., Tytgat, G. & Lightdale, C. *Gastroenterological Endoscopy* (Thieme, 2010).
25. Velitchkov, N. G., Grigorov, G. I., Losanoff, J. E. & Kjossev, K. T. Ingested foreign bodies of the gastrointestinal tract: retrospective analysis of 542 cases. *World J. Surg.* **20**, 1001–1005 (1996).
26. Sandler, R. S., Stewart, W. F., Liberman, J. N., Ricci, J. A. & Zorich, N. L. Abdominal pain, bloating, and diarrhea in the United States. *Dig. Dis. Sci.* **45**, 1166–1171 (2000).
27. Bass, D. M., Prevo, M. & Waxman, D. S. Gastrointestinal safety of an extended-release, nondeformable, oral dosage form (OROS: a retrospective study). *Drug Saf.* **25**, 1021–1033 (2002).
28. Iddan, G., Meron, G., Glukhovsky, A. & Swain, P. Wireless capsule endoscopy. *Nature* **405**, 417 (2000).
29. Hellmig, S. et al. Gastric emptying time of fluids and solids in healthy subjects determined by ^{13}C breath tests: influence of age, sex and body mass index. *J. Gastroenterol. Hepatol.* **21**, 1832–1838 (2006).

30. Wang, Y. R., Fisher, R. S. & Parkman, H. P. Gastroparesis-related hospitalizations in the United States: trends, characteristics, and outcomes, 1995–2004. *Am. J. Gastroenterol.* **103**, 313–322 (2008).
31. Snoeck, V. et al. Gastrointestinal transit time of nondisintegrating radio-opaque pellets in suckling and recently weaned piglets. *J. Control. Release* **94**, 143–153 (2004).
32. Cole, E. T. et al. Enteric coated HPMC capsules designed to achieve intestinal targeting. *Int. J. Pharm.* **231**, 83–95 (2002).
33. Ye, Y., Yu, J., Wen, D. & Kahkoska, A. R. Polymeric microneedles for transdermal protein delivery. *Adv. Drug Deliv. Rev.* **127**, 106–118 (2018).
34. Van Meer, L. et al. Injection site reactions after subcutaneous oligonucleotide therapy. *Br. J. Clin. Pharmacol.* **82**, 340–351 (2016).

Acknowledgements

We thank S. McDonnell, K. Ishida, J. Haupt and M. Jamiel for help with the in vivo porcine work. We thank C. Steiger and Y. L. Kong for helpful conversations on the capsule system. We thank J. Bales and the Edgerton Center at MIT for providing a high-speed camera setup. We thank A. Hupalowska for illustrations of the LUMI concept. We thank the Koch Institute for Integrative Cancer Research at MIT's Histology Core, High Throughput Facility and Imaging Core. We thank the National Disease Research Interchange for help with the procurement of human cadaveric tissue. We thank U. Stilz, M. Bielecki, T. Kjeldsen, L. F. Iversen, J. Trosborg, P. Herskind, R. K. Kirk, F. Hubálek, J. J. Water, A. V. Friderichsen, S. Buckley, A. Vegge and T. B. Pedersen for helpful discussions throughout the development of the LUMI. We are grateful to R. Yona and all of the other members of the Langer and Traverso laboratories and Novo Nordisk for their expertise and discussions around biologic drug delivery. This work was funded in part by a grant from Novo Nordisk and NIH grant number EB000244. A.A. was supported in part by the NSF Graduate Research Fellowship Program fellowship. G.T. was supported in part by the Division of Gastroenterology at Brigham and Woman's Hospital and the Department of Mechanical Engineering at MIT. D.D. was supported by the MIT Undergraduate Research Opportunities Program. N.R. was supported in part by the Viking Olof Björk scholarship trust. H.-C.L., T.Y. and J. Fujimoto were supported in part by NIH R01-CA075289-21.

Author contributions

A.A. and E.C.-S. designed the study, performed the experiments, analyzed and interpreted the data, and wrote the manuscript. V.S., D.M., X.L., R.Y.T., D.D., Y.G., S.K., J.W., J. Fels, M.R.F. and N.R. designed, fabricated and evaluated the prototypes of the system. J.C., S.T. and A.H., designed, performed and helped to analyze the in vivo evaluation of the system. T.Y., H.-C.L. and J. Fujimoto designed, performed and interpreted the characterization of the prototype tissue interactions. U.R., R.L. and G.T. designed, supervised and reviewed the data, and edited the manuscript.

Competing interests

A.A., E.C.-S., D.D., N.R., M.R.F., Y.G., R.L. and G.T. are co-inventors on multiple patent applications describing oral biologic drug delivery. J. Fels, M.R.F. and U.R. work for Novo Nordisk. A.A., R.L. and G.T. report having received consulting fees from Novo Nordisk. A.A. reports having received consulting fees from Eli Lilly. Complete details of all relationships for profit and not for profit for G.T. can found at https://www.dropbox.com/sh/szi7vnr4a2ajb56/AABs5N5i0q9AfT1IqIJAE-T5a?dl=0. For a list of entities with which R.L. is involved (compensated or uncompensated), see https://www.dropbox.com/s/yc3xqb5s8s94v7x/Rev%20Langer%20COI.pdf?dl=0.

Additional information

Extended data is available for this paper at https://doi.org/10.1038/s41591-019-0598-9.

Supplementary information is available for this paper at https://doi.org/10.1038/s41591-019-0598-9.

Correspondence and requests for materials should be addressed to R.L. or G.T.

Peer review information Brett Benedetti was the primary editor on this article and managed its editorial process and peer review in collaboration with the rest of the editorial team.

Reprints and permissions information is available at www.nature.com/reprints.

Publisher's note Springer Nature remains neutral with regard to jurisdictional claims in published maps and institutional affiliations.

Methods

Materials. Dulbecco's phosphate-buffered saline was purchased from Gibco by Life Technologies. Human insulin was obtained from Novo Nordisk. Soluplus was purchased from BASF. The 100,000 and 200,000 molecular weight PEO, along with the sulforhodamine 101 acid chloride (Texas Red), triethyl citrate, talc, acetone, isopropanol, lysozyme from chicken egg, potassium phosphate monobasic solution, potassium phosphate dibasic solution, potassium hydroxide, HCl, *Micrococcus lysodeikitcus* lyophilized cells, bicinchoninic acid kit, α-glucosidase from *Saccharomyces cerevisiae* and α-glucosidase activity assay were purchased from Sigma–Aldrich. Polyvinylpyrrolidone, with an average molecular weight of 58,000, was obtained from Alfa Aesar. Compressed nitrogen gas was purchased from Airgas. Polydimethylsiloxane (PDMS) Sylgard 184 was purchased from Dow Corning. Female Yorkshire swine were obtained from Tufts University, and excised swine tissue was from the Blood Farm slaughterhouse. Cadaveric human tissue was provided within 24 h of retrieval by the National Disease Research Interchange. The Blue CDI's Tissue Marking Dye was purchased from Cancer Diagnostics. Mediprene 4410-LP11L was obtained from Lubrizol. Eudragit L 100-55 and Eudragit S100 were obtained from Evonik. Finally, 316 Stainless Steel Shim Stock was obtained from McMaster-Carr.

Statistical analysis. No data were excluded from the analysis. Student's *t*-tests and area-under-the-curve calculations were performed using Prism Version 7.0 (GraphPad) or Microsoft Excel (Microsoft). A value of $P < 0.05$ was considered statistically significant. All figure captions describe the numbers and types of replicates used in the studies. All figure captions define the center line and error bars used in the plots. All data generated and/or analyzed during the current study are available in the main text, extended data, online methods, source data and supplementary information.

LUMI opening geometric analysis. A geometric analysis of the unfolding event defined a minimum arm length required to provide tissue stretch from any possible orientation. We assumed that the small intestine possessed a known diameter (d), and that the tissue was not rigid. The LUMI device could open up in any orientation, including axially symmetric, parallel, or anywhere in between. An analysis of all of the possible orientations showed that the tissue would stretch the least in the configuration where the planes perpendicular to the central axis containing an arm's point of contact were spaced furthest apart. In this orientation the device opened in a plane parallel to the central axis of the small intestine, as shown in the parallel deployment picture in Fig. 1b. When deployed in this orientation, the arms contacted the tissue over the greatest possible surface area. Because this orientation stretched the tissue the least, we concluded that if the LUMI stretched the tissue in this orientation, it would stretch the tissue in any other possible orientation.

During ex vivo and in vivo studies, we noticed that the small intestine conformed to the LUMI and changed shape. When the LUMI device unfolded in the parallel direction, the tissue transformed from a cylinder and collapsed into two parallel rectangular sheets. If the tissue did not stretch at all in the vertical direction due to the LUMI unfolding event, each of these sheets would be of equal surface area. Because the surface area of the small intestine remained constant, the side length of this newly created rectangle sheet equaled half of the small intestine's perimeter ($\pi d/2$).

Next, we took into account the relationship between the LUMI arm length and the rectangular side length. Each LUMI arm is angularly positioned exactly 120° away from its neighboring arms. Therefore, we know that the height of the triangle created by the tips of each LUMI arm corresponds to 1.5× the LUMI arm length. We also know that the LUMI unfolding position that creates the least amount of stretch in the small intestine occurs when the LUMI opens in a position where the height of the triangle is in the same direction as the side length of the rectangular sheet created by the tissue. To ensure that the tissue stretched, the LUMI triangle height needed to exceed the rectangle side length. Therefore, we determined that the arm length needed to exceed $\pi d/3$ to force the small intestine to stretch when the LUMI opened. In vivo experiments (Fig. 1j) confirmed that LUMIs designed with arms of at least this length were able to stretch the small intestine tissue.

In this particular analysis, we did not take into account the ability of the tissue to conform around the LUMI arm and allow the microneedles to make contact with the tissue; however, we have extensive data that show the ability of the tissue to conform to the microneedle patch on the LUMI, regardless of deployment orientation. In the parallel orientation, the microneedle patch is in the same plane as the tissue; therefore, there is no need to conform to the tissue. The tissue conforming issue would be maximized at the axial configuration, as this is the configuration where the LUMI arm is oriented the furthest from the plane of the tissue. As shown in Fig. 2c and Extended Data Figs. 6 and 7, the tissue allows for microneedle engagement and penetration when the LUMI is deployed in the axial state. Deployment angles in between the parallel and axial state would require less tissue conformation than the axial state deployment angle, and are therefore not an issue due to the experiments performed under axial deployment. To further confirm this, LUMI devices were deployed randomly in vivo, and the conformation of the tissue around the LUMI arm's tip was noted. This experiment was performed concurrently with the experiment performed to acquire the data for Fig. 1i.

LUMI fabrication. Three-dimensional (3D) LUMI models were designed in SolidWorks (Dassault Systèmes) and printed out on an Objet30 Pro 3D printer (Stratasys). A negative mold was created out of PDMS (see Extended Data Fig. 2). Stainless steel cores milled on an Othermill V2 (Bantam Tools) were encased in Mediprene and added to the center core of the mold. A mixture of 25% Soluplus and 75% PEO 200 kDa was microcompounded on an Xplore twin-screw microcompounder (Xplore Instruments) at 50 r.p.m. This mixture was added to the arm sections of the mold. Using a Master-Mite model 10008 heat gun (McMaster-Carr), the materials were melted in the mold. The metal core was aligned to the center of the device. Pressure was then applied to the mold, and the materials were allowed to cool.

Fabricated microneedle patches were then placed on the recessed sections of the LUMI arms. The base plates of the patches were sanded down to a thickness of ≤1 mm, and the patches were cut into 4 × 8 arrays of drug-loaded microneedles. The arms of the device were then reheated using a heat gun, and the patches were placed into the melted recessed sections of the arms.

Tissue perforation characterization. All animal experiments were approved by, and performed in accordance with, the Committee on Animal Care at MIT. Single hypodermic needle perforation testing in vivo was performed by affixing a needle to a 10-N Shimpo force gauge. The force gauge was attached to an arm on a custom stage. We used a motor to move the arm downwards at a rate of 0.2 mm s^{-1}. We placed a camera on the moving stage to visualize the penetration event. The force measurements and video feed were recorded in LabVIEW (National Instruments). In a non-survival experiment, we sedated Yorkshire swine, as described in the in vivo section, and performed a laparotomy procedure to access the small intestine. A 5-cm incision was made in the small intestine to reveal a working area of 5 cm × 1.5 cm, and the tissue was fixed so that it was held taut. The needle was then placed directly over the tissue and moved downward at the defined rate until we were able to visualize the needle on the other side of the tissue. All perforation events were correlated to a force drop. Breathing affected intraoperative measurements, and we determined that the displacement caused by the breathing accounted for an extra 3 mm of penetration. We measured this distance change using a ruler, and confirmed it by analyzing the force versus displacement curves. We confirmed that forces during the exhaled state were equivalent to forces during the inhaled state 3 mm earlier.

Single hypodermic needle perforation testing ex vivo was performed using an Instron 5943 machine equipped with a 10-N load cell. Harvested tissue was affixed to a corkboard with a 2.5-cm-diameter hole. Needles were fixed to the Instron machine's cross-head and lowered into the tissue above the hole at a rate of 0.1 mm s^{-1} until we visualized the needle on the other side of the tissue. All perforation events were correlated to a force drop.

LUMI arm dissolution characterization. Mixtures of either 100 or 200 kDa PEO and Soluplus were combined in an Xplore twin-screw microcompounder (Xplore Instruments) at 50 r.p.m. The extruded material was captured in an Xplore 5.5 cm^3 laboratory injection molding machine and molded into an equilateral triangular prism with side lengths of 3.6 mm and a height of 18.55 mm. The machine exerted 3 bars of pressure for 1 s, ramped up to 4.5 bars over 1 s, and held a pressure of 4.5 bars for an additional 5 s.

Simulated intestinal fluid (SIF) was made by mixing 6.8 g potassium phosphate monobasic (Sigma–Aldrich) with 0.896 g NaOH (Sigma–Aldrich) in 1 l Nanopure Water. The pH was confirmed to be at 6.8 using the Mettler Toledo FiveGo pH meter.

Eight 250-ml Falcon tissue culture flasks (Corning) were labeled and used to house each mixture. A volume of 225 ml of SIF was inserted into each flask and stored at 37 °C in an Innova 44 incubator (Eppendorf) that was shaken at 50 r.p.m. The 50 r.p.m. agitation simulated the intestinal environment. The flasks containing only SIF were left in the incubator for 6 h to allow for temperature equilibration. One extruded shape was dropped inside each flask. The shapes were photographed at the 0-, 1.67- and 22.5-h time points, and appearances of the arms and the SIF were noted (see Extended Data Fig. 4).

Additionally, the mechanical properties of the PEO and Soluplus mixtures were determined during the dissolution process. Using the same microcompounding and extrusion method as described above, bars of the mixtures measuring 3.2 mm × 12.8 mm × 63.5 mm were created. Three-point bend tests were performed on the bars using a uniaxial mechanical tester (Instron 5943). These bend tests were performed on bars that were not placed in any liquid bath, as well as bars that were placed in a shaken and incubated mixture of SIF for 10 min. Bars were fixed on a three-point bend fixture (Instron), with support pins placed 36 mm apart. The cross-head was moved at a rate of 10 mm min^{-1}. The maximum flexural strength was calculated from the maximum load using the following equation:

$$\sigma = \frac{3FL}{bd^2}$$

where F is the load at the fracture point, L is the length of the support span, b is the width of the bar, and d is the thickness of the bar. The maximum flexural strength for the LUMI arm was also calculated from this equation using the arm's dimensions.

Optimizing the arm force on the tissue. Varying the arm length and unfolding angle affected the amount of force delivered by the LUMI arm (Fig. 1f,k; see Extended Data Fig. 2). Devices with longer arms required less angular expansion before making contact with tissue compared with devices with shorter arms. The core, consisting of a 76-µm-thick spring steel shim stock embedded in Mediprene elastomer, delivered a greater amount of force at more acute unfolding angles.

The addition of the steel piece also increased the contact force between the arm and the impact point. This effect was not seen if the Mediprene material continued along the arm past the steel section. For example, in a 15-mm-long Mediprene core with a 7-mm-long steel section, there existed no significant change in contact force between a device with the steel part and one without (Fig. 1f). In an 8-mm-long core, adding the 7-mm-long, 76-µm-thick steel resulted in a 60% increase in the contact force. Adding the steel piece also increased the force exerted for a 45° deflection and a 180° torsion by 150 and 50%, respectively (Fig. 1g,h). Steel pieces thinner than 0.076 mm commonly broke after multiple tests, and those thicker commonly ruptured the Mediprene coating.

In vivo, we tested the ability for LUMI devices with different arm lengths and cores to stretch the tissue. Devices oriented in all directions provided at least some tissue stretch, but axially oriented devices provided more stretch than parallel oriented devices. We noted that devices with 25-mm-long arms oriented in the axial direction after opening more frequently than devices with 23-mm-long arms (Fig. 1i). We also noted that devices with 25-mm-long arms containing a metal core oriented axially more frequently than those without a metal core. Axially oriented devices stretched the tissue to a diameter of 40 mm at the tissue's narrowest point in the plane perpendicular to the tissue's central axis. Devices containing metal cores provided a greater tissue stretch than devices with cores that did not include metal when orienting in the parallel direction. These devices stretched the tissue to 12 and 10 mm, respectively (Fig. 1j). Adding metal to the core also increased the likelihood of axial deployments because the increased force required for deflection limited the device's flexibility to change conformations.

Capsule fabrication. Three-dimensional models of the capsule pieces were created in SolidWorks and printed on an Objet30 Pro 3D printer. The two body portions of the capsule were adhered together by spray coating Eudragit S100 onto the piece as they were clasped together. Eudragit spray coating was performed per the published Evonic guidelines. To create the mixture, 342.9 g acetone, 514.2 g isopropanol and 42.9 g water were combined. Then, 62.50 g of the Eudragit polymer was added to 50% of the diluent mixture and stirred for 60 min. At the same time, 6.25 g triethyl citrate and 31.25 g talc were added to the remaining diluent mixture and stirred for 10 min. The excipient suspension was then added to the Eudragit suspension, stirred for 5 min, then passed through a 0.5-mm sieve. The combined solution was spray-coated using a Master Economy E91 Single-Action airbrush set with a 0.8-mm tip and a 3.175-mm air inlet (TCP Global). The inlet stream was pressurized with compressed nitrogen to 0.1 MPa. The spray-coating process yielded a coating at least 20 µm thick. The capsule piece holding the spring was press fit into one portion of the capsule's body. A spring with a compressed length of 4.1 mm, a load of 1.3 N and a free length of 31.8 mm (Spring CI 011EF 11S; Lee Spring) was then trimmed to a length of 30 mm and cut in half. Using thread (SparkFun), one half of the springs were tied to one section of the capsule, and the other half were tied to the plunger. The two spring halves were then placed inside the capsule in series. Pressure was applied on the plunger to fully compress the spring. Melted PEG was then fed through the capsule to freeze the spring in place. Molecular weights of PEG between 3,000 and 35,000 were used. The change in dissolution time allowed the capsule to release the device at different time intervals. The relationship between PEG's molecular weight and capsule actuation was tested in a bath of SIF heated to 37 °C. Eudragit L 100-55 was then spray-coated onto that section of the device to coat the PEG using the same method described previously. The LUMI device was then placed inside the capsule, and the cap was put onto the other side of the capsule.

Capsule deployment. The capsule was designed to actuate after leaving the stomach and entering the duodenum. A Eudragit L 100-55 (poly(methacrylic acid-co-ethyl acrylate)) coating designed to dissolve at a pH of ≥5.5 (a value experienced in the duodenum but not in the stomach[35]), dissolved after being in the environment of the small intestine and exposed two holes on one end of the capsule. The efficacy of the pH-sensitive coating was verified in vitro by placing the capsules in buffers of increasing pH, starting at pH 2. X-ray imaging confirmed that capsule actuation occurred within 2 h of residing in the small intestine in vivo (Fig. 1c). Importantly, the capsule possessed two chambers. One section was waterproof and contained the LUMI device while the other possessed a moisture- and pH-activated actuation mechanism made from a PEG-encapsulated compressed spring and a pH-sensitive poly(methacrylic acid-co-ethyl acrylate) coating. Exposing the holes allowed fluid to access the inside of the capsule's spring chamber. This fluid then started to dissolve the PEG coating encasing the two compressed springs in series. Once dissolved, the springs propelled the LUMI device out of the capsule by pushing on a plunger inside the capsule (Fig. 1a). In vitro, we demonstrated that changing the capsule actuation mechanism allowed the capsule to actuate over different time scales from 1.5–5.0 h after entering an environment with a pH of >5.5 (Fig. 1l). In their expanded state, each spring measured ≤15 mm in length. The ends of the springs were capped with a polycaprolactone coating to prevent them from perforating the intestinal wall. One spring was tied to the base of the capsule using SparkFun conductive thread (SparkFun) so that it would remain inside the capsule walls as it passed through the gastrointestinal tract. The other spring was tied to the plunger via two holes placed on the bottom of the plunger, using the same conductive thread. After the LUMI device was released, it unfolded and delivered the microneedle patches to the intestinal wall. The elastomeric core of the LUMI exited the capsule last, protecting the microneedles from shearing or compressing against the capsule structure.

Just as the LUMI arms were designed to reduce intestinal obstructions, the capsule was also constructed to mitigate this potential complication. After the LUMI device was ejected, the same holes used to allow fluid to dissolve the actuation mechanism permitted the passage of intestinal fluid through the capsule. Additionally, we fabricated the capsule so that the walls consisted of multiple pieces no larger than 9 mm in diameter and 15 mm in length (Fig. 1e). The wall pieces were held together via a pH-sensitive polymer coating, which dissolved at ≥pH 7.0—a value generally observed in the lower intestine but not in the upper portion of the small intestine[35]. We demonstrated in vitro that the coating kept the capsule intact during device actuation, yet within 2 h after entering an environment with a pH >7, the capsule broke into multiple pieces. We verified that coated capsules delivered in vivo to swine lost mechanical integrity at this junction point by retrieving and inspecting them post-excretion.

Microneedle fabrication. Positive microneedle master molds with varying microneedle heights were obtained from Novo Nordisk Devices and were machined out of 304 stainless steel. Negative molds were then fabricated by pouring PDMS over the positive master molds and baking them at a temperature of 60 °C for 24 h. The molds used for the LUMI device created microneedles with a height of 1 mm and a base diameter of 0.4 mm. Microneedles with heights varying from 600–1,200 µm were also fabricated and tested for their ability to penetrate swine small intestine tissue (Extended Data Fig. 7a), but they were not used with the LUMI device.

Microneedle patches were fabricated with insulin concentrated in the tips. Solid insulin powder was placed in PDMS female microneedle molds and forced into the microneedle tips using a spatula. Excess powder was then removed from the mold. The amount of powder added to the mold was calculated by weighing the mold before and after the addition of powder. The accuracy of weight measurements was confirmed using high-performance liquid chromatography. Briefly, we employed a 7.8 × 300 mm^2 insulin HMWP column (Waters), set to room temperature, and an Agilent high-performance liquid chromatography machine. Elutions were performed at a flow rate of 0.5 ml min^{-1} for 26 min using a mobile phase made from 15% acetic acid (*v*/*v*), 20% acetonitrile (*v*/*v*) and 0.65 g l^{-1} L-arginine, all purchased from Sigma–Aldrich. The molds were then centrifuged at 3,200 RCF for 10 min to compress the powder. Next, a 50% 58,000 molecular weight polyvinylpyrrolidone solution in deionized water or 100% sorbitol was added to bind the powder and give mechanical structure to the microneedle patches. The mold was then centrifuged again at 3,200 RCF for 10 min. The microneedle patches were left to dry at room temperature for 72 h. Once dried, microneedle patches were unmolded, sanded down and mounted onto the recessed edges of the LUMI arms. We loaded 0.3 mg insulin per LUMI. The amount of API could be increased by further compressing the powder into the microneedles. A maximum insulin load of 0.5 mg per LUMI could be achieved.

The microneedles made from lysozyme and α-glucosidase were fabricated in the same manner. The amount of protein in the tips of these microneedle patches was determined via a bicinchoninic acid assay. The activity of lysozyme, either in the microneedle formulation or as a lyophilized powder, was measured by analyzing the cell lysis of *M. lysodeikitcus*, per the protocol published by Sigma–Aldrich. The activity of α-glucosidase, either in the microneedle formulation or as a lyophilized powder, was evaluated using an activity assay kit that measured the hydrolysis of *p*-nitrophenyl-α-D-glucopyranoside. The activity of the proteins (U mg^{-1}) in the patches were then compared with the activities of the unformulated, lyophilized proteins to determine their stability in the formulations.

LUMI fabrication for potential high-throughput production. LUMI fabrication began with the core, which was milled to shape. In a scaled-up process, the metal core could be stamped using a steel die. The next step was encapsulating the core with an elastomer. To fabricate proof-of-concept LUMI cores, we cast two halves of the elastomeric core, then placed the metal core between each half, and re-melted the cores together. This casting and re-melting process could be replaced with an over-mold injection molding process around the steel core. In the laboratory setting, the LUMI arms were fabricated by microcompounding Soluplus and PEG together and casting the mixture to shape. The microcompounding could be scaled up, and the casting could be replaced with injection molding. Each of the injection molding steps could be executed in series in an assembly line, and overmolding techniques could be used to join each component. The LUMI microneedles were solvent casted. This process is being scaled up commercially for the purpose of transdermal drug delivery, and a similar process would be used during scaled-up LUMI manufacturing. The microneedles could be attached to the LUMI arms using a snap fit, press fit or other locking mechanism during the scaled-up process.

During our proof-of-concept study, the capsule pieces were 3D printed, but these pieces could be injection molded in a commercial setting. Assembly of the capsule pieces could be performed using one of the locking mechanisms described above. The spring and the LUMI device could be placed inside the capsule during the assembly process. Fixing of the compressed spring was performed in the study by casting the spring inside the capsule; during scale-up, this process could be performed using injection molding to cast the spring. Coating of the capsule in an enteric polymer was performed using a spray coat process, and this process could be scaled up in a commercial setting.

Microneedle dissolution. Microneedle dissolution patterns and, in turn, drug-delivery kinetics were studied using both insulin and Texas Red-based fluorescent dyes. Microneedles loaded with Texas Red and Texas Red conjugated with dextran (3 kDa) were used to perform dissolution tests both in vivo in swine before euthanasia and ex vivo in human small intestinal tissue. Microneedles were manually inserted for 5, 15 and 30 s, then retrieved. A microneedle patch (0.30 g) was left to sit on top of the tissue without applying any external pressure for 30 s, which served as the negative control. An in vivo imaging system (Perkin Elmer) was then used to assess the Texas Red and Texas Red–dextran transfer onto the tissue via fluorescence. Living Image software (Perkin Elmer) was used to quantify the radiant efficiency. The same dissolution kinetics occurred when measuring dye transfer from microneedle patches to both ex vivo human tissue and in vivo swine tissue (Fig. 2d,f; see Extended Data Fig. 9d). Over a 30-s time period, the inserted microneedles transferred twice as much dye to the tissue and six times as much insulin to the gel on average compared with the negative control.

Microneedle penetration. A 1.3-μm-wavelength OCT system developed at MIT and optical microscopy were used to visualize penetration of the microneedles into excised small intestines from swine (Fig. 2i; see Extended Data Fig. 8). For this, various microneedle arrays were inserted ex vivo into the tissues via manual application, and OCT was used to evaluate both the penetration depth and dissolution. In addition, a fixture (see Extended Data Fig. 7) was designed to hold the LUMI and deploy one of its arms at a 30° angle into a certain point of an ex vivo swine small intestine piece, to promptly capture the penetration event before microneedle dissolution. In this latter case, the OCT image was captured from the outside of the tissue wall instead of from behind the patch, allowing the assessment of perforation. OCT images were processed using Image J (Open Source).

Penetration of the microneedles attached to the LUMI into small intestine tissue was also tested by performing histology and microCT on ex vivo swine tissue. MicroCT imaging was performed on a GE CT120 microCT imaging system (General Electric). The devices were deployed with either sharpened metal hypodermic needles or microneedles loaded with barium sulfate (Sigma–Aldrich). The needles were also coated in a tissue-marking dye (Cancer Diagnostics), to mark the area of tissue penetration for histology.

In vivo testing. All animal experiments were approved by, and performed in accordance with, the Committee on Animal Care at MIT. To assess the insulin microneedle formulation, we administered the API formulation to female Yorkshire swine of 35–65 kg. To deliver the LUMI devices, we placed the swine on a liquid diet for 24 h before the procedure, and fasted the swine overnight. We then sedated them with an intramuscular injection of Telazol (tiletamine/zolazepam) (5 mg kg^{-1}), xylazine (2 mg kg^{-1}) and atropine (0.05 mg kg^{-1}), along with supplemental isoflurane (1–3% in oxygen) via a face mask. An orogastric tube or overtube was placed with the guidance of a gastric endoscope, and remained in the esophagus to facilitate the passage of the device. The overtube was passed through the stomach and into the small intestine. Encapsulated LUMI devices were passed through the overtube and placed into the small intestine. Non-encapsulated LUMI devices were inserted and actuated during a non-survival procedure, whereby a ventral midline laparotomy was performed to access the small intestine. A 3-cm incision was made in the intestinal wall to access the mucosa. During these non-survival experiments, the size of the small intestine was standardized to 20 mm in diameter by applying a clamp to the tissue. The microneedles delivered manually to the small intestine were also inserted during a similar laparotomy procedure, during which a 3-cm incision was used to access the small intestinal mucosa, and a microneedle patch was manually inserted into the intestinal surface epithelium. Patches with an area of 1 cm^2 were applied to the jejunum of the swine. Pressure was applied to the patch for 30 s, then the patch was removed from the small intestine. To create the subcutaneous dose required for administration, the microneedles from four patches were dissolved into 2 ml sterile saline (Hospira). The mixture was then filtered through an Acrodisc 0.2-μm low protein binding filter (Pall Life Sciences), and 0.5 ml of the resulting solution was administered to each swine subcutaneously. Lastly, the insulin solution dosed to the jejunum was prepared by dissolving the microneedles from one patch into 10 ml water purified using a Barnstead Nanopure system (Thermo Fisher Scientific). The solution was then passed through an endoscope directly into the jejunum of the swine.

We obtained blood samples via a central venous line at time points including (but not limited to) every 10 min for the first 2 h, and every 30 min for hours 2–4. We immediately tested the blood samples for glucose levels using a OneTouch Ultra glucose monitor by LifeScan. Blood glucose level changes were recorded over 4 h, and dextrose was administered when hypoglycemia was observed. We collected additional blood into ethylenediaminetetraacetic K3 tubes (Sarstedt), and spun them down at 2,000 RCF for 15 min. Collected plasma from MIT was shipped on dry ice to Novo Nordisk in Måløv, Denmark, and blood was analyzed there via an AlphaLISA developed at Novo Nordisk. Briefly, the homogenous bead assay employed two monoclonal antibodies against human insulin, creating acceptor-bead, insulin and donor-bead layering. This generated a signal that was proportional to the concentration of insulin. Additionally, blood was analyzed at MIT using an enzyme-linked immunosorbent assay developed at Novo Nordisk. Both tests utilized antibodies specific for human insulin, and neither test detected other endogenous insulins.

Figure 4a, for purposes of clarity, shows only a few representative time points from the pharmacokinetics curve collected during the experiments. However, Fig. 4c uses all time points collected when determining the area under the curve calculation. All data from the in vivo pharmacokinetics experiments can be found in the source data file for Fig. 4. In Fig. 4c and Supplementary Table 2, the area under the curve was calculated by an algorithm in Prism 7.04 software using the following parameters: a y baseline of 0; an exclusion of peaks less than 10% of the distance from the minimum to the maximum y value; and an inclusion of all peaks regardless of whether or not they were defined by a single outlying point. In Fig. 4c, we calculated individual area under the curve computations for each animal and represented them as single data points. In Supplementary Table 2, we used the combined data set of all three animals in an experimental group to determine the average and standard error for the area under the curve of each experimental group. Of note, in the experimental group receiving the intestine gavage of dissolved microneedles, all time-point samples that showed human insulin in the animal's blood plasma had adjacent time-point samples showing no human insulin in the blood plasma. We included these uptake peaks generated from the described data points in the analysis in Fig. 4c and Supplementary Table 2, and confined these individual peaks to match an area under the curve measurement over a peak time frame of 15 min or less. This time frame is equivalent to two to three half-lives of human insulin. If peaks that were defined by three or fewer points were not included in these calculations—meaning that the peaks described above made from only one outlying point and two zero points were excluded—then the swine receiving the intestinal gavage of dissolved microneedles would have shown no human insulin uptake; on the other hand, the swine dosed with human insulin via the LUMI, intestine microneedle patch, or subcutaneous injection of dissolved microneedles would have shown only a 6%, 2%, and <1% difference, respectively, compared to the numbers reported in the calculations for Fig. 4c and Supplementary Table 2. Depending on the methods used to calculate the area under the curve, different confidence intervals comparing the experimental groups can be inferred. Future efforts toward successful human translation should aim to expand experimental replicates in pigs and likely dogs to increase our understanding of the pharmacokinetic variability associated with the intestinal delivery methods used in this study. Specialized LUMI devices were administered to the swine to determine the capsule actuation time as well as the transit and dissolution timeline for the LUMI. These LUMI devices contained small pieces of metal material, such as nitinol or stainless steel, which allowed the device to be seen when radiographed. The swine were radiographed over several hours in the case of the capsule actuation experiments. The swine were radiographed over several days in the case of the transit experiments until all of the metal components had passed through the gastrointestinal tract. For the transit experiment, we collected the cage shavings and searched for the devices. Some of the devices were lost in the cage shavings, but at least one device per animal was recovered. We confirmed that all of the devices passed through the body by euthanizing the swine and performing an examination of the entire gastrointestinal tract.

When taking histology, animals were sacrificed 5–15 min after the delivery events so that an entire cross-section of tissue could be examined at the exact point of device deployment. Tissue-marking dye was used to denote the appropriate area for histology. Redness and bleeding were observed at the tissue sites of microneedle insertion immediately after LUMI deployment and the direct insertion of microneedles, signifying tissue penetration. These phenomena rapidly disappeared within minutes, as confirmed via visual inspection of the tissue.

Reporting Summary. Further information on research design is available in the Nature Research Reporting Summary linked to this article.

Data availability

The data supporting the findings of this study are available within the paper and its Supplementary Information files.

References

35. Fallingborg, J. Intraluminal pH of the human gastrointestinal tract. *Dan. Med. Bull.* **46**, 183–196 (1999).

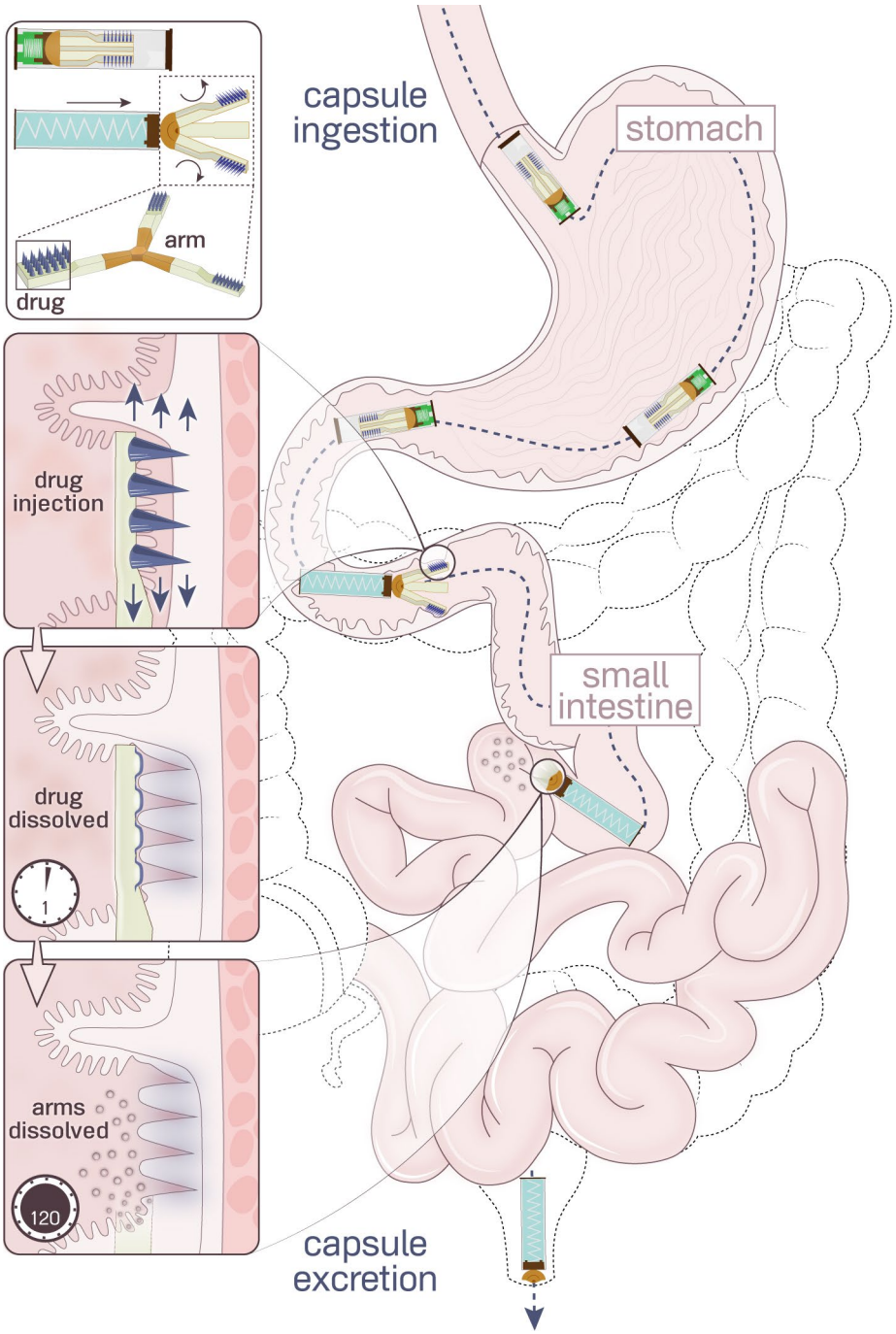

Extended Data Fig. 1 | Luminal Unfolding Microneedle Injector (LUMI) schematic timeline. LUMI devices were administered in enteric capsules. They actuated and unfolded in the small intestine, injecting drug loaded microneedles into the tissue wall. The microneedle patches and arms dissolved within several hours. The non-degradable parts of the device passed through the gastrointestinal tract and were excreted.

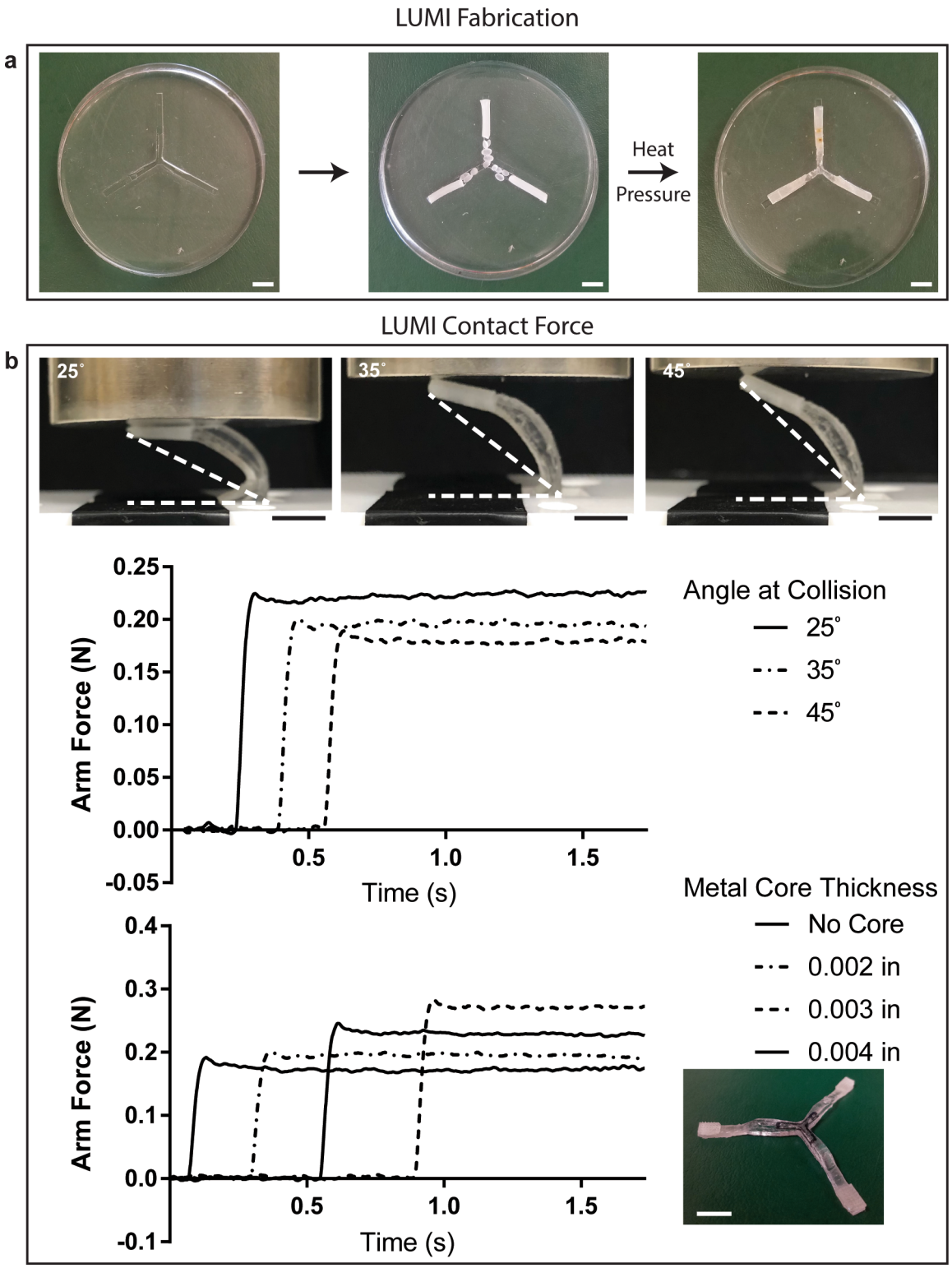

Extended Data Fig. 2 | LUMI Fabrication Scheme and Generated Contact Forces. a, Custom fabricated PDMS mold for creation of LUMI backbone. Metal cores were embedded in the elastomer during heating. **b**, Force applied to a steel compression platen by LUMI arm over time after actuation. (n = 1 representative device replicate). Scatter plots of the data are shown in Fig. 2f. Scale bars = 1 cm.Source data

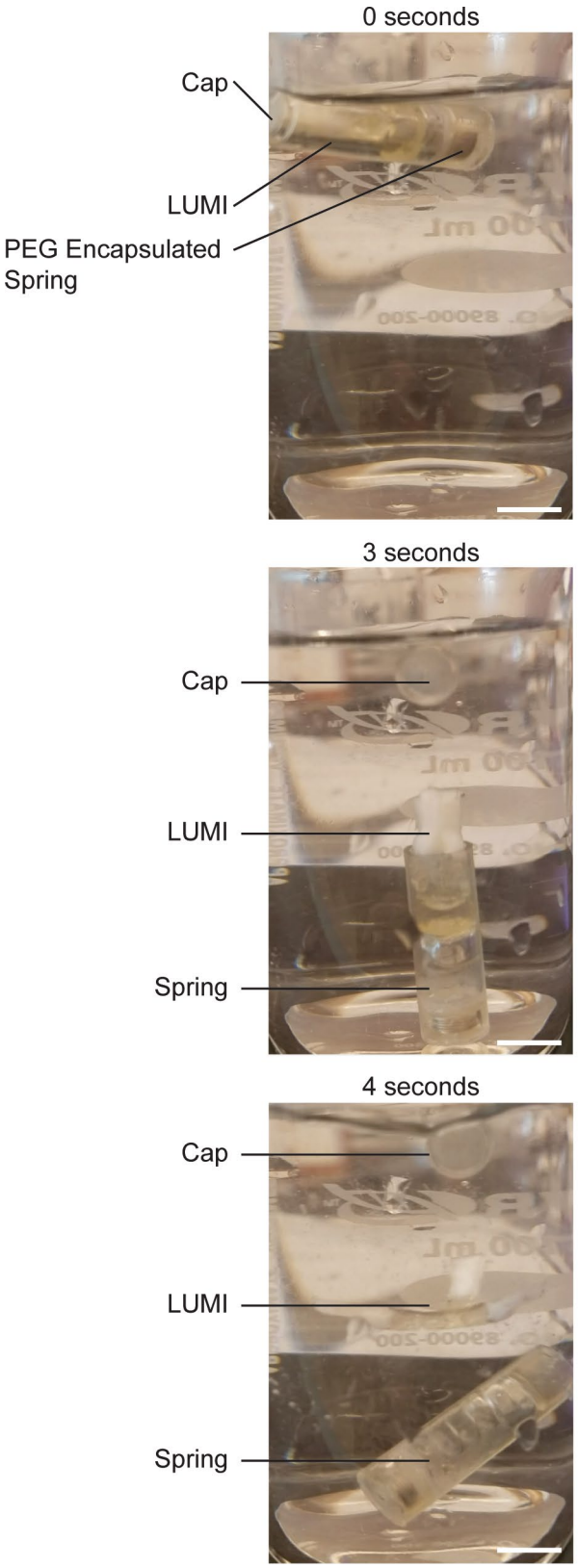

1. The watertight capsule containing the LUMI floats on top of the water due to air encapsulated around the LUMI. Water begins to dissolve the PEG encapsulating the compressed spring.

2. After the PEG dissolves, the spring begins to expand. This causes the cap of the capsule to pop off. Water fills the capsule after the cap is ejected, causing the entire capsule to sink.

3. The LUMI is expelled from the capsule and unfolds due to the stored energy in the elastomeric core.

Extended Data Fig. 3 | Prototype watertight capsule demonstration in water. The LUMI is protected from external liquid until immediately before it unfolds. Before the actuation occurs, the PEG must dissolve over a period of 1–5 h. Scale bars = 1 cm.

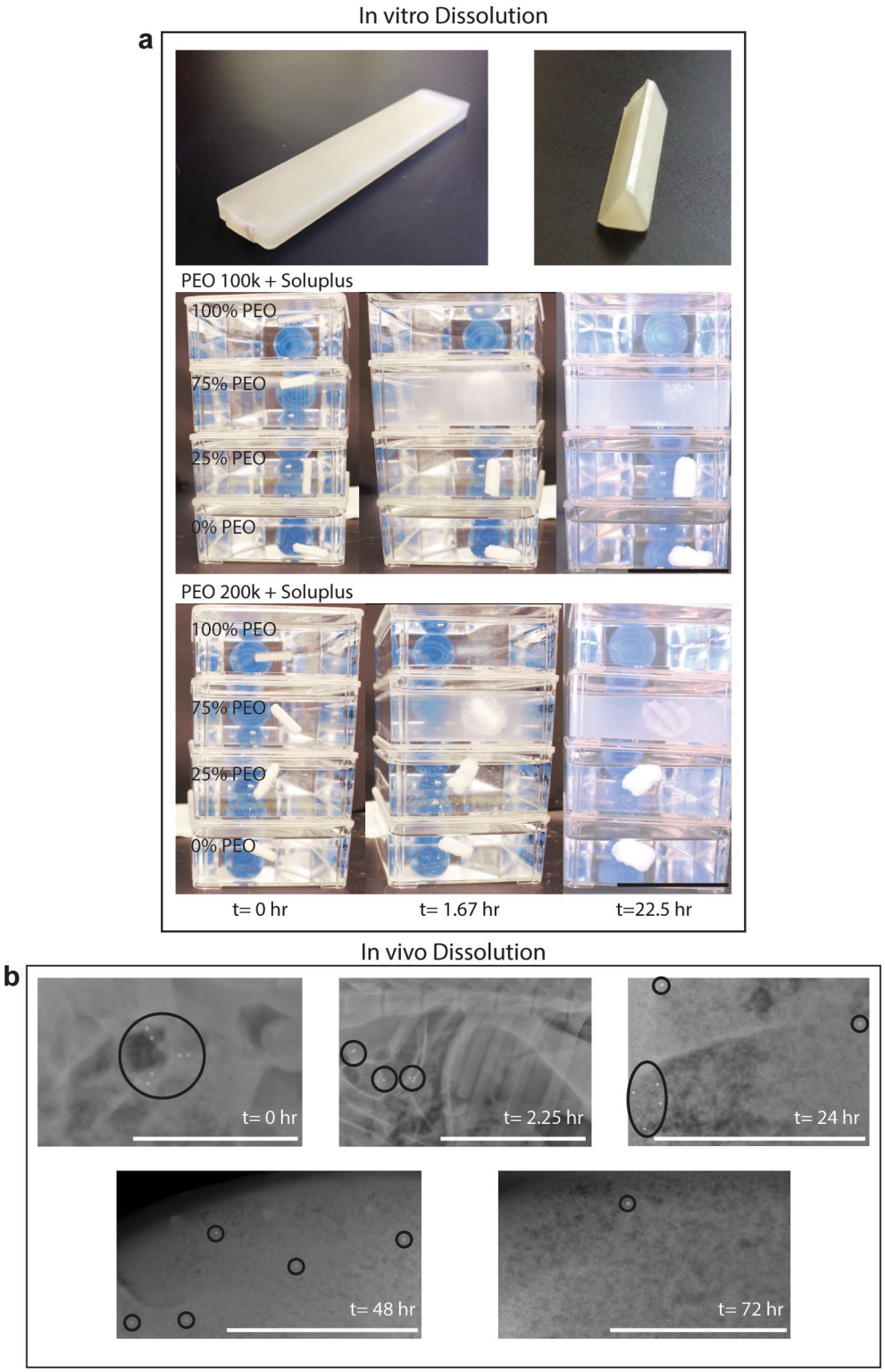

Extended Data Fig. 4 | In vitro and in vivo LUMI dissolution. a, Bar (3.2 × 12.8 × 63.5 mm) and arm (3.6 mm equilateral triangle side length, 18.6 mm length) shapes used for flexural strength and dissolution testing respectively. Dissolution of arm shapes over time *in vitro* at 37 °C in simulated intestinal fluid is shown. Scale bars = 5 cm. **b**, A LUMI device is delivered to the small intestine in an enteric capsule and degrades over time. Stainless steel ball bearings 1 mm in diameter are placed on the arms to aid in visualization. The metal beads served as radio-opaque fiducials and were not part of the final design. Scale bars = 5 cm.

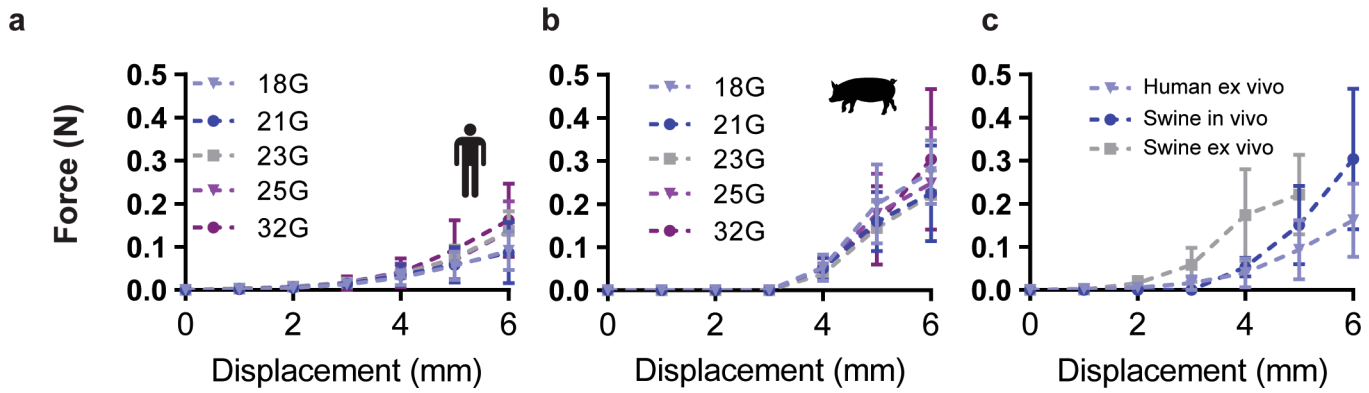

Extended Data Fig. 5 | Penetration characterization for small intestine tissue. Forces required for needle displacement in (**a**) *ex vivo* human and (**b**) *in vivo* swine small intestine tissue, respectively. (**c**) A comparison between human and swine forces in the small intestine using 32 G needles. (Ex vivo tissue: n = 4–5 technical replicates each for 2 animal/patient replicates totaling n = 9–10; In vivo tissue: n = 5 technical replicates each for 3 animal replicates totaling n = 15. Error bars = SD. Center dot = mean.)Source data

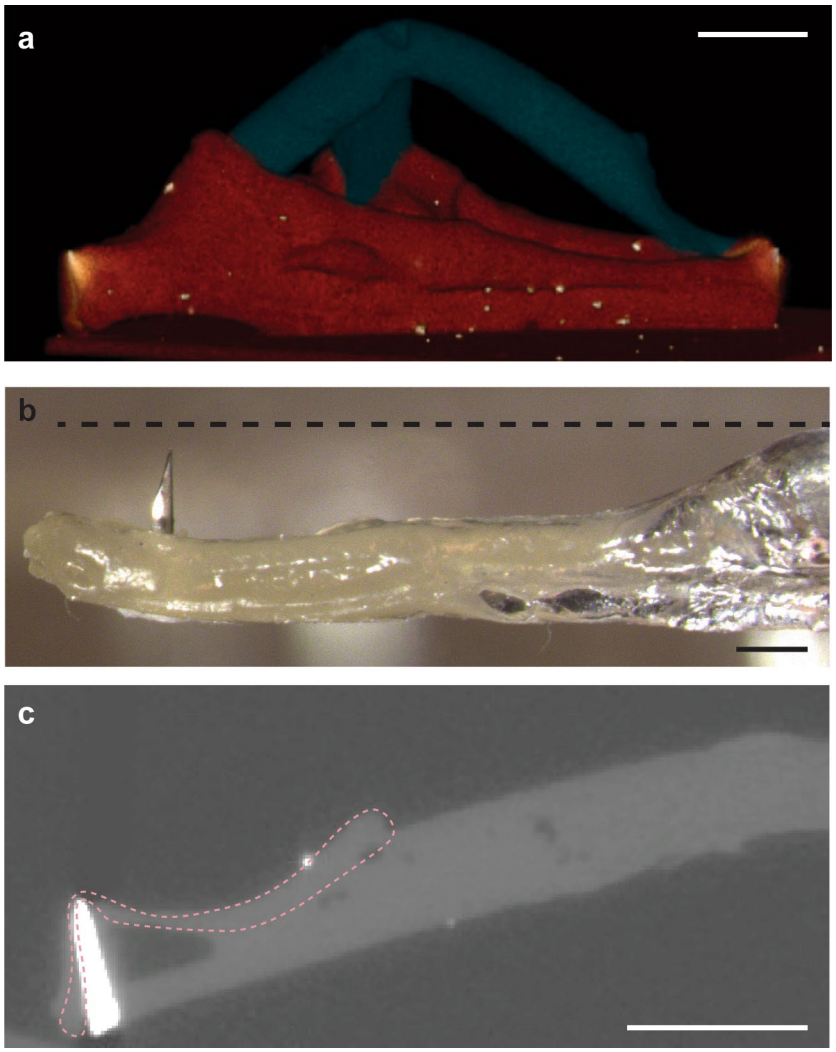

Extended Data Fig. 6 | LUMI deployment with hypodermic needle. a, Colored MicroCT reconstruction. Scale bar = 10 mm. **b**, Needle is same height as microneedles. Scale bar = 1 mm. **c**, MicroCT cross section of LUMI deployment. Tissue is outlined. Scale bar = 5 mm.

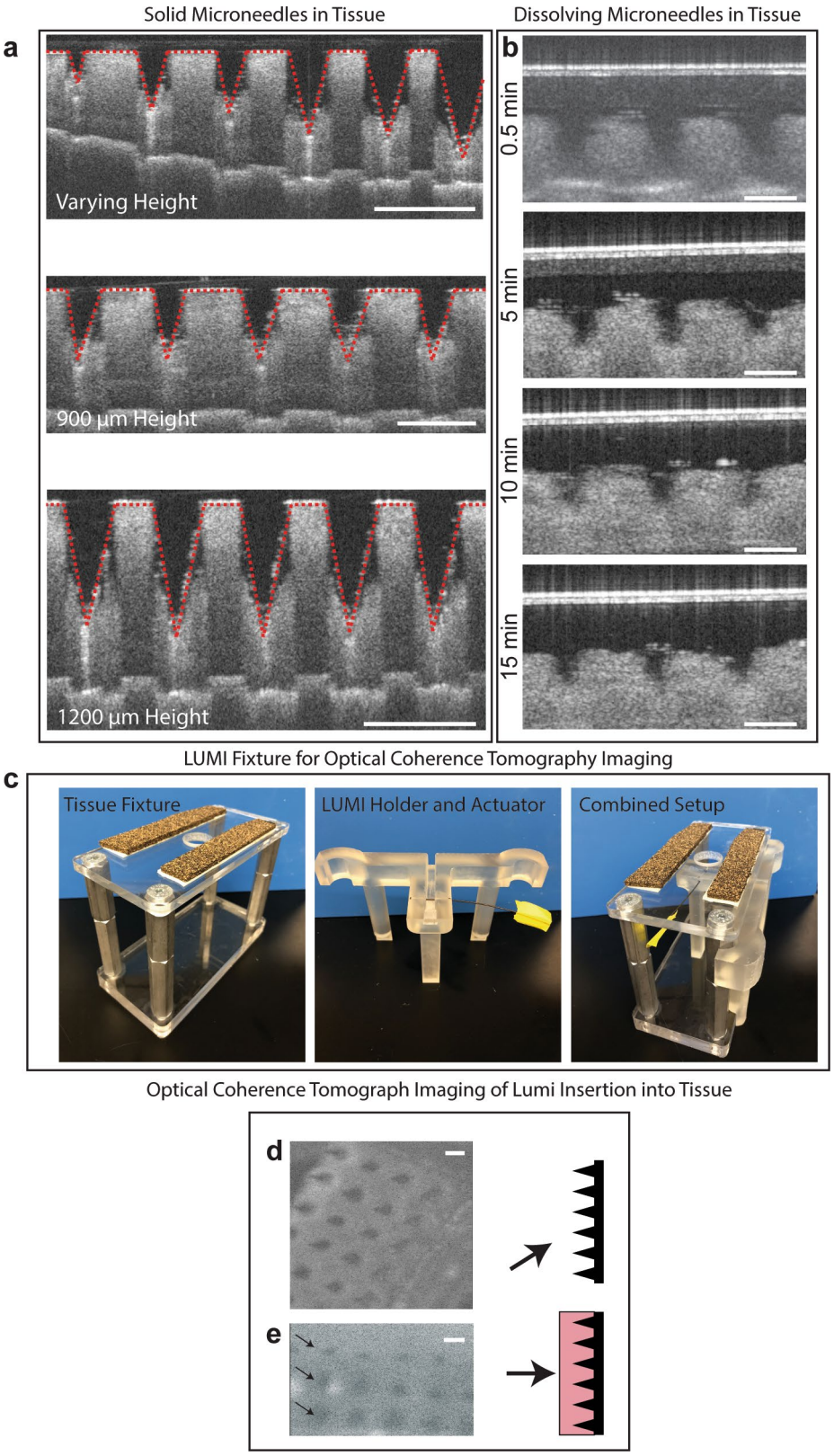

Extended Data Fig. 7 | Optical coherence tomography (OCT) images of microneedle penetration. a, **b**, OCT imaging showing (**a**) solid microneedles (Scale Bars = 1 mm) and (**b**) dissolving microneedle patches in *ex vivo* swine tissue (Scale bars = 0.5 mm). **c**, Fixture used to deploy LUMI during OCT imaging. Tissue holder dimensions are: 65 mm L x 140 mm W x 106 mm H. LUMI actuator dimensions are 67 mm L x 155 mm W x 93 mm H. **d**, **e**, OCT images showing the microneedles mounted in the LUMI arm (**d**) prior to insertion and (**e**) inserted into small intestine after deploying the arm from a 30 degree angle (Scale bars = 0.5 mm). Arrows in **e** point to the holes observed in the tissue corresponding to microneedles being inserted. The differences in the holes' size reflect the different penetration depths from tilted insertion. Animations to the right denote the angle of the imager compared to the microneedle patch on the LUMI arm.

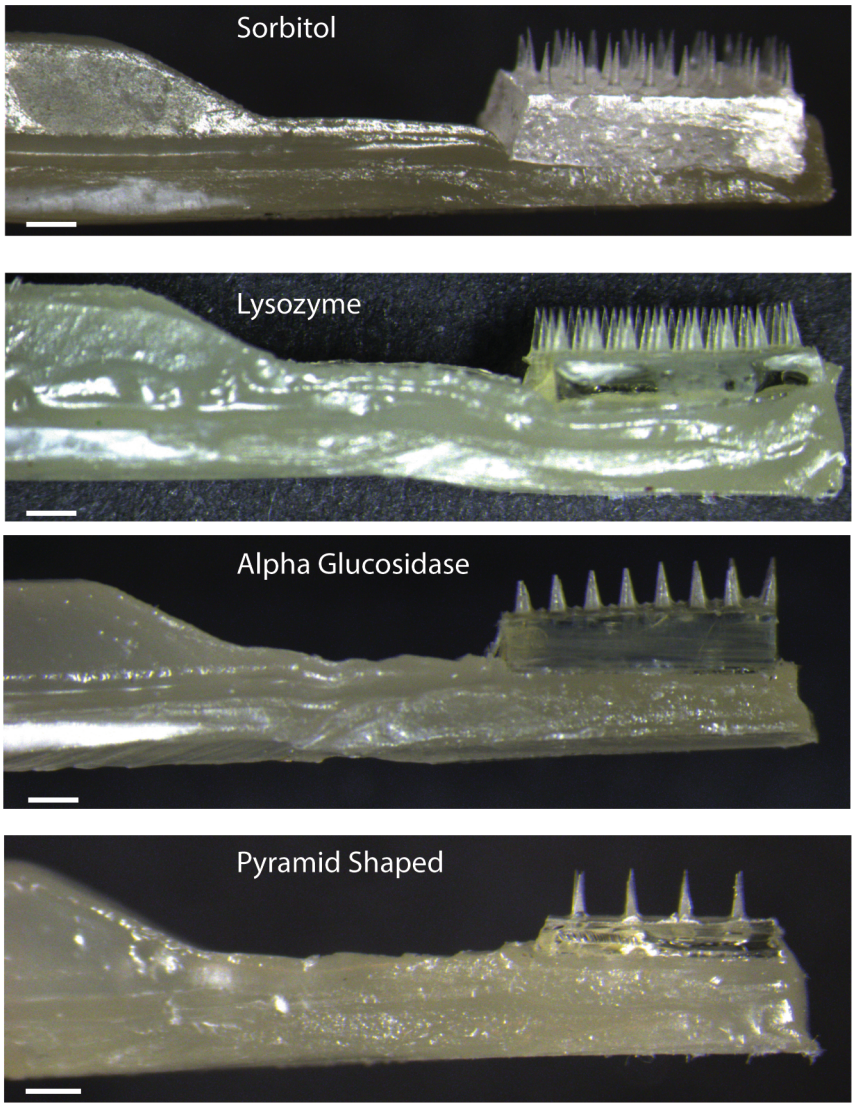

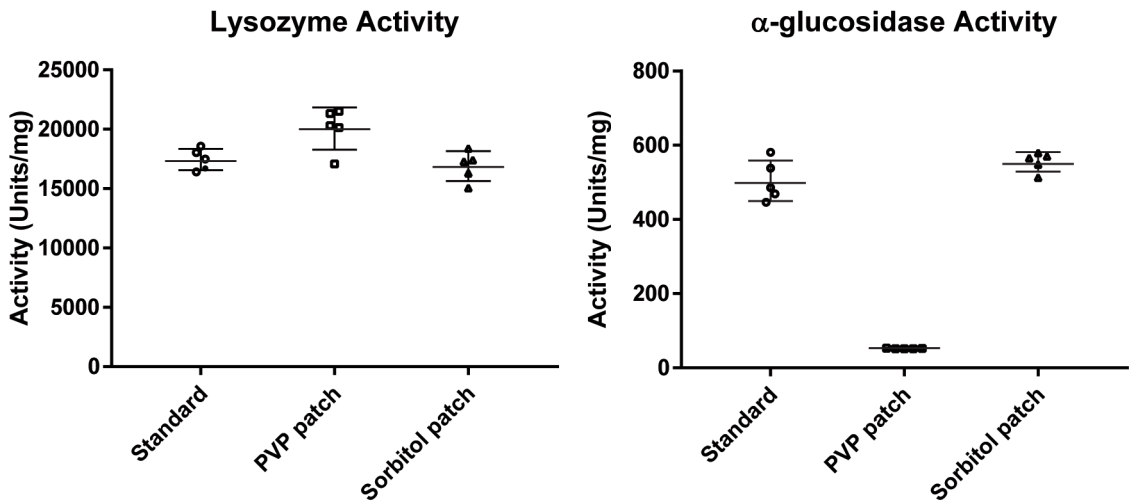

Extended Data Fig. 8 | LUMI devices made with various excipients and biomacromolecules. LUMI arms with microneedle patches made with different formulations and active pharmaceutical ingredient are pictured. Aside from the sorbitol patch, all patches use polyvinylpyrrolidone (PVP) as a binding agent. Activity of lysozyme and alpha-glucosidase in microneedle formulations are shown. Scale bars = 1 mm. (n = 5 device replicates. Error Bars = SD. Center line = mean.)Source data

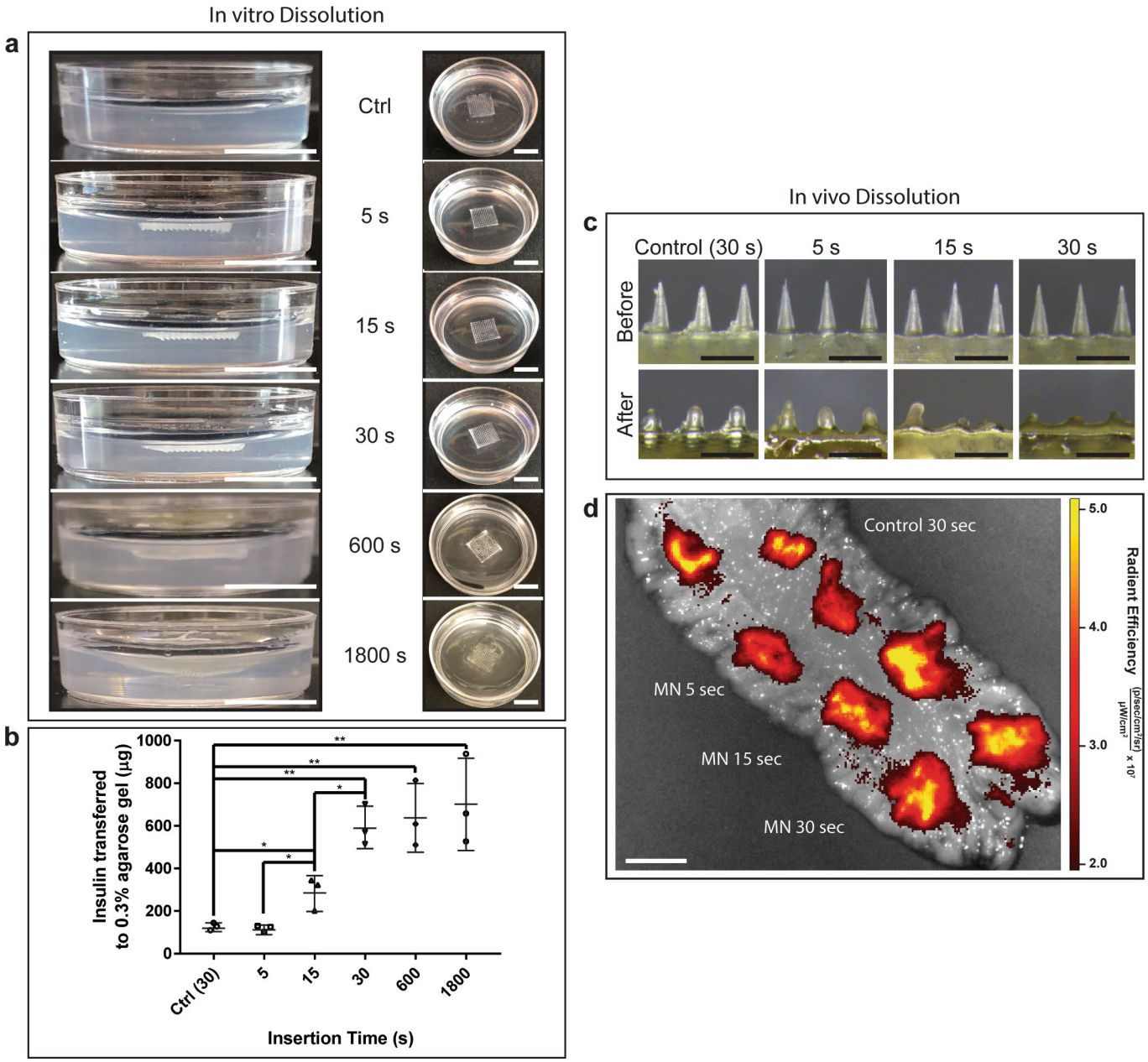

Extended Data Fig. 9 | In vitro and in vivo microneedle dissolution and macromolecule transfer. a, Insulin microneedle patch dissolution in 0.3% agarose gel. Patches which were inserted into the gel for a set period of time were compared to patches which were laid on top of the gel for 30 s (control). The figure includes views of the gel from the side (left) and top (right) after the patch was removed. Scale bars = 1 cm. **b**, Insulin transferred from the patch to the gel quantified via HPLC. (n = 3 device replicates. Error Bars = SD. Center line = mean. *P < 0.05, **P < 0.01). **c**, Dissolution of insulin microneedle patches after application to *in vivo* swine small intestine. Control patches were laid upon the tissue and all other patches were penetrated into to the tissue. Scale bars = 1 mm. **d**, In vivo imaging system fluorescent image of swine tissue applied with Texas red loaded microneedle patches. Patches were applied *in vivo*. The control patches were left to sit on top of the tissue, but they were not pressed into the tissue. Scale bar = 1 cm.Source data

nature research

Corresponding author(s): Robert Langer
Giovanni Traverso

Last updated by author(s): Aug 22, 2019

Reporting Summary

Nature Research wishes to improve the reproducibility of the work that we publish. This form provides structure for consistency and transparency in reporting. For further information on Nature Research policies, see Authors & Referees and the Editorial Policy Checklist.

Statistics

For all statistical analyses, confirm that the following items are present in the figure legend, table legend, main text, or Methods section.

n/a	Confirmed	
☐	☒	The exact sample size (*n*) for each experimental group/condition, given as a discrete number and unit of measurement
☐	☒	A statement on whether measurements were taken from distinct samples or whether the same sample was measured repeatedly
☐	☒	The statistical test(s) used AND whether they are one- or two-sided *Only common tests should be described solely by name; describe more complex techniques in the Methods section.*
☐	☒	A description of all covariates tested
☐	☒	A description of any assumptions or corrections, such as tests of normality and adjustment for multiple comparisons
☐	☒	A full description of the statistical parameters including central tendency (e.g. means) or other basic estimates (e.g. regression coefficient) AND variation (e.g. standard deviation) or associated estimates of uncertainty (e.g. confidence intervals)
☐	☒	For null hypothesis testing, the test statistic (e.g. *F*, *t*, *r*) with confidence intervals, effect sizes, degrees of freedom and *P* value noted *Give P values as exact values whenever suitable.*
☒	☐	For Bayesian analysis, information on the choice of priors and Markov chain Monte Carlo settings
☒	☐	For hierarchical and complex designs, identification of the appropriate level for tests and full reporting of outcomes
☒	☐	Estimates of effect sizes (e.g. Cohen's *d*, Pearson's *r*), indicating how they were calculated

Our web collection on statistics for biologists contains articles on many of the points above.

Software and code

Policy information about availability of computer code

Data collection	No code was used for data collection
Data analysis	Prism and Microsoft Excel Were used to analyze data

For manuscripts utilizing custom algorithms or software that are central to the research but not yet described in published literature, software must be made available to editors/reviewers. We strongly encourage code deposition in a community repository (e.g. GitHub). See the Nature Research guidelines for submitting code & software for further information.

Data

Policy information about availability of data

All manuscripts must include a data availability statement. This statement should provide the following information, where applicable:

- Accession codes, unique identifiers, or web links for publicly available datasets
- A list of figures that have associated raw data
- A description of any restrictions on data availability

The authors declare that the data supporting the findings of this study are available within the paper and its supplementary information files.

Field-specific reporting

Please select the one below that is the best fit for your research. If you are not sure, read the appropriate sections before making your selection.

☒ Life sciences ☐ Behavioural & social sciences ☐ Ecological, evolutionary & environmental sciences

For a reference copy of the document with all sections, see nature.com/documents/nr-reporting-summary-flat.pdf

Life sciences study design

All studies must disclose on these points even when the disclosure is negative.

Sample size	For in vivo studies, initial proof-of-concept sample size was guided by our prior work with gastric devices.
Data exclusions	No data was excluded
Replication	Multiple tests were taken on different days and using different animals or tissue to ensure that the data was reproducible.
Randomization	No randomization, not reported
Blinding	No blinding, not reported

Reporting for specific materials, systems and methods

We require information from authors about some types of materials, experimental systems and methods used in many studies. Here, indicate whether each material, system or method listed is relevant to your study. If you are not sure if a list item applies to your research, read the appropriate section before selecting a response.

Materials & experimental systems

n/a	Involved in the study
☐	☒ Antibodies
☒	☐ Eukaryotic cell lines
☒	☐ Palaeontology
☐	☒ Animals and other organisms
☐	☒ Human research participants
☒	☐ Clinical data

Methods

n/a	Involved in the study
☒	☐ ChIP-seq
☒	☐ Flow cytometry
☒	☐ MRI-based neuroimaging

Antibodies

Antibodies used	Anti Human Insulin antibody was used in the elisa assay. This was custom made by Johannes Fels at Novo Nordisk
Validation	A validation of the specificity of antibody binding to human insulin over all other types of animal insulin and other proteins was performed and is published in DOI: 10.1126/science.aau2277

Animals and other organisms

Policy information about studies involving animals; ARRIVE guidelines recommended for reporting animal research

Laboratory animals	Female Yorkshire Swine, aged 6 months to 1 year
Wild animals	None used
Field-collected samples	none collected
Ethics oversight	MIT committee for animal care

Note that full information on the approval of the study protocol must also be provided in the manuscript.

Human research participants

Policy information about studies involving human research participants

Population characteristics	Post mortem human tissue samples were collected by NDRI. A table of the exact patient characteristics is provided in Table 1 of the manuscript.
Recruitment	Post mortem human samples were collected by the NDRI and shipped on ice to MIT. The samples were used within 24 hours after collection and did not need to be stored.
Ethics oversight	Because the samples were collected postmortem the researchers received an exemption form from the MIT Committee on the Use of Humans as Experimental Subjects

Note that full information on the approval of the study protocol must also be provided in the manuscript.